# *Chapter 4: Preparation, antibody conjugation and characterization of nanoparticles*
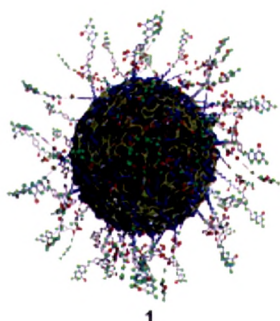
1

4. PREPARATION, OPTIMIZATION, ANTIBODY CONJUGATION AND CHARACTERIZATION OF NANOPARTICLES

Various disorders of the brain require drug delivery to the brain for treatment. However, such transport remains problematic especially for hydrophilic and large molecular weight molecules, due to the presence of Blood–Brain Barrier (BBB) (Pardridge 1999). Hence, many therapeutic agents have been abandoned because of insufficient levels in the brain through the systemic circulation. Intranasal administration is a rapidly budding strategy to deliver drugs noninvasively and effectively to the brain. Various strategies have been tried to potentially improve direct nose to brain delivery of drugs including proteins one of which is drug encapsulation into particulate vectors such as synthetic nanoparticles (Zhang et al 2006, Csaba et al 2009). Nanotechnology is an area of science devoted to the manipulation of atoms and molecules leading to the construction of structures in the nanometer scale size range (often 100 nm or smaller), which retain unique properties. Types of nanoparticulate vectors include liposomes, nanoparticles, micelles, etc. There is an increased interest in developing biodegradable nanoparticles owing to their low toxicity profiles and offer a suitable means of delivering small molecular weight drugs, proteins or genes by localized or targeted delivery to the tissue of interest (Moghimi et al 2001, Feng 2004). Amongst these nanoparticulate delivery systems polymeric nanoparticles have shown promising properties for targeted drug delivery and for sustained action. These include polymers like polyepsilon caprolactone (PCL), poly (lactide-co-glycolide) (PLGA) and poly lactic acid (PLA), etc. (Langer 1997, Jain 2000). Nanoparticles contain therapeutic agents entrapped in, adsorbed or chemically coupled onto the polymer matrix (Labhasetwar 1997).

Nanoparticles can be prepared by polymerization of monomers entrapping the drug molecules leading to insitu polymerization or from preformed polymers. Several techniques have been suggested to prepare the biodegradable polymeric nanoparticles from preformed polymers such as poly (D, L-lactide) {PLA}, poly (D, L-glycolide) {PGA} and poly (D,L-lactide-co-glycolide) {PLGA}. Various methods proposed for the preparation of PLGA nanoparticles include emulsification/solvent evaporation, solvent displacement/diffusion (nanoprecipitation), emulsification/solvent diffusion

and salting out using synthetic polymers (Quintanar-Guerrero et al 1998). Emulsification solvent evaporation technique is one of the fastest methods for nanoparticle preparation and is readily scalable. Emulsification solvent evaporation is a two-step process: the emulsification of a polymer solution containing the encapsulated substance, followed by particle hardening through solvent evaporation and polymer precipitation. During emulsification, the polymer solution is broken up into nanodroplets by the shear stress produced either by homogenizer, sonicator or whirl mixer in the presence of a surface-active agent. This first step mainly determines the size and size distribution of nanoparticles. In the present investigation, Lutrol F-68 was used as an emulsifier and PVA as a stabilizer to form nanoparticles of relatively small size and uniform size distribution (Sahoo et al 2002, Scholes et al 1993).

Various formulation and process variables relating to effectiveness, safety, and usefulness should be optimized simultaneously when developing pharmaceutical formulations. The difficulties in optimizing a pharmaceutical formulation are due to the difficulty in understanding the real relationship between casual and individual pharmaceutical responses. A factorial design has often been applied to optimize the formulation variables (Misra et al 2002, Levison et al 1994, Shirakura et al 1991). The optimization procedure based on response surface methodology (RSM) includes statistical experimental designs, multiple regression analysis, and mathematical optimization algorithms for seeking the best formulation under a set of constrained equations. Since theoretical relationships between the response variables and causal factors are not clear, multiple regression analysis can be applied to the prediction of response variables on the basis of a second-order equation. In the present study, drug: polymer ratio, Lutrol F-68 concentration and organic phase to aqueous phase ratio were selected as independent variables, whereas particle size and %EE were selected as dependent variables.

Surface modification of PLGA NPs has been attempted by either conjugating their surface with different ligands or conjugating ligands to the polymer followed by preparation of NPs. Ligands which have been reported are folic acid (Stella et al 2000), transferrin (Sahoo et al 2004), biotin (Minko 2004), lectins (Sharma et al 2004), antibodies (Aktas et al 2005, Kocbek et al 2007), etc. These ligands bind

specifically to the receptors on the plasma membrane of the target tissue which leads to the internalization of plasma membrane receptors along with the delivery system i.e. NPs.

The surface modification of PLGA nanoparticles by the active ester method yields stable amide bonds. As a prerequisite, the polymer has to contain free carboxyl groups at the surface as represented by the H-type of PLGA which are activated by carbodiimide/N-hydroxysuccinimide. In contrast to the activation of carboxyls with only carbodiimide, the presence of N-hydroxysuccinimide yields N-hydroxysuccinimide esters as stable intermediates which rather acylate amino groups of proteins than to be subject of hydrolysis in aqueous medium (Staros et al 1986, Grabarek et al 1990). Additionally, the activation and coupling can be performed at neutral pH.

Characterization of the nanoparticles is essential to understand their properties before putting them to pharmaceutical application. After preparation, nanoparticles are characterized at two levels. Physicochemical characterization consists of the evaluation of the particle size, size distribution and surface properties (composition, charge, hydrophobicity) of the nanoparticles. The biopharmaceutical characterization includes measurements of drug encapsulation, in vitro drug release rates, and in vivo studies revealing biodistribution, bioavailability, and efficacy of the drug.

There are many sensitive techniques for characterizing nanoparticles, depending upon the parameter being looked at; laser light scattering (LLS) or photon correlation spectroscopy (PCS) for particle size and size distribution; scanning electron microscopy (SEM), transmission electron microscopy (TEM), and atomic force microscopy (AFM) for morphological properties; X-ray photoelectron spectroscopy (XPS), Fourier transform infrared spectroscopy (FTIR), and nuclear magnetic resonance spectroscopy (NMR) for surface chemistry; and differential scanning calorimetry (DSC) for thermal properties.

Parameters such as density, molecular weight, and crystallinity affect release and degradation properties, where as surface charge, hydrophilicity, and hydrophobicity significantly influence interaction with the biological environment.

112

Dichloromethane (DCM) and chloroform belongs to class 2 solvents which should be limited due to potential toxicity. Limit for DCM is 600ppm and for chloroform is 60ppm and their permissible daily exposure is 6mg/day and 0.6mg/day respectively (ICH guidelines). These were analyzed as per USP method using gas chromatography coupled with static head space sampling.

Table 4.1 Materials and equipments

Material	Source
Nicergoline	Gift samples from Ivax Pharmaceuticals s.r.o, Opava-Komarov, Crech Republic.
Hydergine	Gift samples from Ivax Pharmaceuticals s.r.o, Opava-Komarov, Crech Republic.
Sibutramine Base (SB)	Extracted from SBHM Gift sample from Matrix Laboratories Ltd., Secunderabad, India.
Water (distilled)	Prepared in laboratory by distillation
PLGA (50:50)	Gift samples from gift sample from Boehringer Ingelheim, Germany
Lutrol F-68	Gift sample from BASF, Germany
Polyvinyl alcohol (PVA, mol wt 30000-70000; hydrolyzed 87-89%)	Sigma Chemicals, India
Phycoerythrin tagged anti-CD71 anti-mouse monoclonal antibody (PE-mAb-Tfr)	Santa Cruz Biotechnology, Inc. U.S.A.
1-Ethyl-3-[3-dimethylaminopropyl] carbodiimide hydrochloride (EDC or EADC hydrochloride), N-hydroxysuccinimide and HEPES buffer	Himedia Laboratories Pvt. Ltd., Mumbai, India
Glycine	Sisco Research Laboratories Pvt. Ltd., Mumbai, India
Potassium dihydrogen phosphate, disodium hydrogen phosphate, potassium chloride, potassium hydroxide, sodium chloride, sodium hydroxide	S.D. Fine chemicals, India
HPLC grade methanol, acetonitrile, dichloromethane, chloroform.	S.D. Fine chemicals, India
Nuclepore Polycarbonate membrane 2 μm 25mm	Whatman, USA

Equipments	Source/Make
Calibrated pipettes of 1.0 ml, 5.0 ml and 10.0 ml, volumetric flasks of 10 ml, 25 ml, 50 ml and 100 ml capacity, Funnels (i.d. 5.0 cm), beakers (250 ml) and other requisite glasswares	Schott & Corning (India) Ltd., Mumbai

Analytical balance	AX 120, Shimadzu Corp., Japan
pH meter	Pico$^+$ Labindia, Mumbai, India
Spinix vortex shaker	Durga corporation, Gujarat, India
Cyclomixer, magnetic stirrer	Remi Scientific Equipments, Mumbai, India
Cooling Centrifuge	3K 30, Sigma Laboratory centrifuge, Osterode, GmBH.
Lyophilizer	DW1, 0-60E, Heto Drywinner, Denmark
Stability oven	Shree Kailash Industries, Vadodara
Spectrofluorophotometer	Shimadzu RF-540, equipped with data recorder, Japan
UV-Visible Spectrophotometer	Shimadzu UV-1601, Japan
Vacuum Pump F16	Bharat Vacuum pumps, Bangalore
Magnetic stirrer	Remi Instrument Ltd., India
Bath sonicator	Ultra Sonic, Trans-O-Sonic, India
Probe sonicator	Labsonic M, Sartorius AG, Germany
Malvern particle size analyser	Malvern zeta sizer NanoZS, U.K.
Transmission electron microscope	Morgagni, Philips, Netherlands
Differential Scanning Calorimeter	Mettler DSC 20, Mettler Toledo, Switzerland
^{1}H-NMR	av300, Bruker, UK

4.1 Methods

4.1.1 Precipitation of sibutramine base (SB) from Sibutramine hydrochloride monohydrate (SBHM) salt

Sibutramine hydrochloride monohydrate (SBHM) salt was dissolved in sufficient distilled water in a separating funnel. This aqueous phase was basified with 0.5N sodium hydroxide till it turns milky due to the liberation of free sibutramine base. The liberated base was then extracted using triple volume of chloroform (in fractions) compared to aqueous phase. The organic phases were mixed together and allowed to evaporate till completely dry. When dried, to the precipitated SB water was added to remove any water soluble impurity present, filtered and allowed to dry at ambient conditions. Yield calculated and the resulting solid subjected to melting point and DSC analysis.

4.1.2 Preparation and optimization of nanoparticles

The PLGA nanoparticles of the drugs nicergoline (NNp), sibutramine base (SNp) and hydergine (HNp) were prepared using the simple emulsion solvent evaporation

technique [Guerrero et al 1998]. The process parameters like rate of addition of primary emulsion, the speed of the high speed stirrer (or cyclomixer), the probe sonication time and the stirring time were standardized before proceeding for the optimization of the formulation parameters using nicergoline as model drug and results tabulated in tables 4.3-4.6. The process parameters were standardized taking into account the size and entrapment efficiency of the prepared nanoparticles keeping drug to polymer ratio fixed as 1:15, volume of organic phase as mL/mg solid content, volume of aqueous phase as 30 mL and total concentrations of surfactants Lutrol F-68 as 0.37%w/v and PVA as 0.07%w/v (1.6%w/v Lutrol F-68 and 0.5%w/v PVA for primary emulsion).

Figure 4.1: Schematic representation of emulsion solvent evaporation process
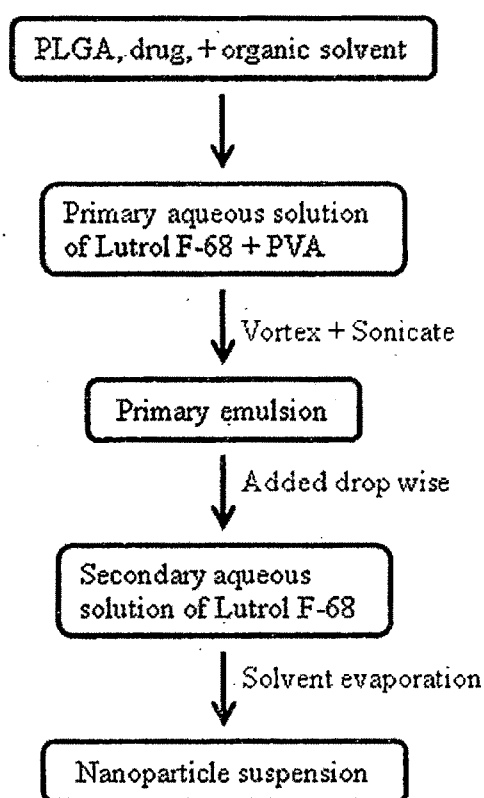
Briefly, the drug and polymer (84mg) were completely solubilized in methylene chloride (for NG and SB) or chloroform (for HG) (1mL) and added to primary aqueous surfactant solution (2.2-3.5mL) containing Lutrol F-68 (1.45-1.75%w/v) and PVA (0.5%w/v). The resulting mixture was vortexed to get a stable primary emulsion which was then sonicated (90 amplitude with 0.6sec interval) for 90 sec. The resulting

emulsion was then diluted drop-wise (1.5mL/min) by injection through 0.2mm needle into an aqueous Lutrol F-68 (0.11-0.14% w/v) solution (26-27mL) with continuous stirring (12,000 rpm) on a high speed stirrer for 30 min (dilution step). PVA was included only to stabilize the primary emulsion formed while within the syringe for secondary dilution and hence, was kept constant for all the three drugs. With the gradual evaporation of solvent from the dispersion, the polymer precipitates leading to formation of nanoparticles. The resulting nanoparticle dispersion was then kept open at ambient conditions overnight for further evaporation of residual organic phase if any. Nanoparticles, NNp, SNp and HNp were then recovered by centrifugation for 15 min at 10000 rpm, washed three times with distilled water to remove unentrapped drug and excess surfactants, and then lyophilized for 24 hrs.

Optimization of formulation parameters

Pharmaceutical formulations are effected by single or combination of variables. It is difficult to assess the effect of the variables individually or in combination. Factorial designs allow all the factors to be varied simultaneously, thus enabling evaluation of the effects of each variable at each level and showing interrelationship among them. Factorial designs are of choice when simultaneous determination of the effects of several factors and their interactions on response parameters is required. A prior knowledge and understanding of the process and the process variables under investigation are necessary for achieving a more realistic model. Initial experiments revealed the critical role of polymer concentration (as drug to polymer weight ratio), surfactant concentration, organic to aqueous phase ratio as major variables in determining the particle size (PS) and percentage drug entrapment efficiency (%EE). Hence, drug to polymer ratio per mL of organic phase (represented as polymer to drug weight ratios), Lutrol F-68 total concentration (i.e in primary + secondary aqueous phase) and organic to aqueous phase volume (represented as primary + secondary aqueous phase volume) were selected as independent variables to find the optimized condition for response variables like particle size (PS) (<225nm, so that after antibody conjugation the PS of nanoparticles resides below 225nm) with highest percentage entrapment efficiency (%EE) using 3^3 factorial design and contour plots. The values of these selected variables along with their transformed values are:

Coded values for the formulation parameters for preparation of nanoparticles

Coded Values	Independent Variables		
	Aqueous Phase volume (X_1)	Lutrol F-68 conc. (%w/v) (X_2)	Polymer to drug weight ratio (X_3)
-1	25	0.27	10
0	30	0.32	20
1	35	0.37	30

* The amount of the drug was fixed at 5mg and the polymer amount was changed

Twenty seven batches of nanoparticles were prepared by emulsion solvent evaporation method according to the 3^3 experimental design shown in table 4.7 for NG, table 4.8 for HG and table 4.9 for SB respectively. The prepared batches were evaluated for particle size, drug entrapment efficiency and the results were recorded in table 4.7 for NG, table 4.8 for HG and table 4.9 for SB respectively.

A multilinear stepwise regression analysis was performed using Microsoft Excel software. Mathematical modeling was carried out by using Equation 1 to obtain a second-order polynomial equation:

$$Y = b_0 + b_1X_1 + b_2X_2 + b_3X_3 + b_{11}X_1^2 + b_{22}X_2^2 + b_{33}X3^2 + b_{12}X_1X_2 + b_{13}X_1X_3 + b_{23}X_2X_3$$
$$+ b_{123}X_1X_2X_3........(\text{Equation 1})$$

Where b_0 is the arithmetic mean response of 27 runs and b_1, b_2 and b_3 is the estimated coefficients for the factors X_1, X_2 and X_3, respectively. The major responses represent the average result obtained by changing one factor at a time from its low to high value. The interactions show the change in particle size when two or more factors are varied simultaneously. The following equations were was derived by the best-fit method to describe the relationship of the particle size (Y_{PS}) and entrapment efficiency (Y_{EE}) with the polymer concentration (X_1), PVA concentration (X_2) and the ratio of org. phase: aq. phase (X_3). A full model was established after putting the values of regression coefficients in Equation 1.

Equations 2 and 3 represent the full model equations for NNp for particle size and entrapment efficiency respectively:

$$Y_{PS} = 181.0195 - 33.3548X_1 - 29.427X_2 + 33.69522X_3 + 4.477004X_1^2 + 17.79367X_2^2$$
$$+ 21.19367X_3^2 + 0.082173X_1X_2 + 6.007173X_1X_3 + 5.440506X_2X_3 + 0.614241X_1X_2X_3$$
$$...(\text{Equation 2})$$

$Y_{\%EE} = 80.79578 - 3.4865X_1 - 2.6365X_2 + 3.796835X_3 - 1.04684X_1^2 - 2.3635X_2^2 - 0.83017X_3^2 - 0.28692X_1X_2 + 0.63808X_1X_3 - 0.29525X_2X_3 - 0.81962X_1X_2X_3$ ....(Equation 3)

Equation 4 and 5 represent the full model equations for HNp for particle size and entrapment efficiency respectively:

$Y_{PS} = 211.7453 - -20.9105X_1 - -42.7827X_2 + 11.73952X_3 + 2.6327X_1^2 + 17.61603X_2^2 - 7.2173X_3^2 - 3.25928X_1X_2 - 0.72595X_1X_3 - 8.66762X_2X_3 + 1.288924X_1X_2X_3$ ......(Equation 4)

$Y_{\%EE} = 64.52264 - 3.18579X_1 - 5.06913X_2 + 3.286428X_3 - 0.62532X_1^2 - 1.54198X_2^2 - 4.44198X_3^2 - 1.17964X_1X_2 - 0.62131X_1X_3 - 0.67964X_2X_3 + 0.856962X_1X_2X_3$ ......(Equation 5)

Equation 6 and 7 represent the full model equations for SNp for particle size and entrapment efficiency respectively:

$Y_{PS} = 214.5001 - 21.9027X_1 - 55.5916X_2 + 16.99733X_3 + 1.091561X_1^2 + 3.158228X_2^2 + 10.02489X_3^2 + 0.704008X_1X_2 + 1.904008X_1X_3 + 1.962342X_2X_3 - 2.10601X_1X_2X_3$ ..(Equation 6)

$Y_{\%EE} = 61.59859 - 1.75105X_1 - 5.88439X_2 + 2.771167X_3 - 0.28228X_1^2 - 1.04895X_2^2 - 1.64895X_3^2 - 0.24842X_1X_2 - 0.22342X_1X_3 - 0.20675X_2X_3 - 0.11487X_1X_2X_3$ ....(Equation 7)

Neglecting nonsignificant (P > 0.05) terms from the full model, a reduced model was established, which facilitates the optimization technique by plotting contour plots keeping one major contributing independent formulation variable constant and varying other two independent formulation variables to establish the relationship between independent and dependent variables.

Equations 8 and 9 represent the reduced model equations for NNp for particle size and entrapment efficiency respectively:

$Y_{PS} = 184.6095 - 32.4469X_1 - 28.5191X_2 + 34.60312X_3 + 16.88577X_2^2 + 20.28577X_3^2$ ....(Equation 8)

$Y_{\%EE} = 79.54444 - 3.46865X_1 - 2.61865X_2 + 3.814683X_3 - 2.38135X_2^2$ ....(Equation 9)

Equation 10 and 11 represent the reduced model equations for HNp for particle size and entrapment efficiency respectively:

Y_{PS} = 208.6889 - 21.4547X_1 - 43.3269X_2 + 11.19533X_3 + 18.16022X_2^2 - 7.85133X_2X_3.......(Equation 10)

$Y_{\%EE}$ = 63.07778 - 3.47579X_1 - 5.35913X_2 + 2.996429X_3 - 4.15198X_3^2 ...... (Equation 11)

Equation 12 and 13 represent the reduced model equations for HNp for particle size and entrapment efficiency respectively:

Y_{PS} = 217.3333 - 21.3056X_1 - 54.9944X_2 + 17.59444X_3 + 9.427778X_3^2 ......(Equation 12)

$Y_{\%EE}$ = 60.31111 - 1.8373X_1 - 5.97063X_2 + 2.684921X_3 - 0.9627X_2^2 ...... (Equation 13)

ANOVA

Analysis of variance (ANOVA) of full model and reduced model was carried out and the F statistic was applied to check whether the nonsignificant terms can be omitted or not, from the full model. Table 4.10 show the results of analysis of variance of full and reduced model for PS and %EE of NG nanoparticles, table 4.11 show the results for HG nanoparticles and table 4.12 show the results for SB nanoparticles.

Construction of contours

Two dimensional contour plots were established using the reduced polynomial equations. At fixed levels of -1, 0 and 1 of independent variable with highest coefficient value, values of independent variables were computed for particle size and entrapment efficiency and contour plots were established The contours for NG, HG and SB are shown in Figures 4.2 to 4.3, Figures 4.4 to 4.5 and Figures 4.6 to 4.7 respectively.

Check Point Analysis

A check point analysis was performed to confirm the utility of established contour plots and reduced polynomial equation in the preparation of etoposide and temozolomide nanoparticles. Values of two independent variables were taken from

three check points each on contour plots plotted at fixed levels i.e -1, 0 and 1 of independent variable of highest coefficient and the values of particle size and entrapment efficiency were generated by NCSS software. Nanoparticles were prepared experimentally by taking the amounts of the independent variables on the same check points. Each batch was prepared in triplicate and mean values were determined and tabulated in table 4.13 for NG, table 4.14 for HG and table 4.15 for SB. Difference of theoretically computed values of particle size and entrapment efficiency and the mean values of experimentally obtained particle size and entrapment efficiency were compared by using student't' test method.

4.2.3 Lyophilization and optimization of cryoprotectant concentration

The nanoparticle dispersions have thermodynamic instability upon storage and lead to the formation of aggregates (Saez et al 2000). Freeze drying/lyophilization is one of the known methods to recover nanoparticles in the dried form and suitably redisperse them at the time of administration. To the suspension of the nanoparticles different cryoprotectants like sucrose, mannitol and trehalose were added in different concentrations at nanoparticle (NP): cryoprotectant (CP) ratio of 1:2, 1:3 and 1:4 before freeze-drying. The effect of these cryoprotectants on the redispersibility and size of the freeze-dried formulations after freeze-drying was investigated using NG nanoparticles and recorded in table 4.16.

4.2.4 Antibody conjugation of nanoparticles

Phycoerythrin-tagged-anti-mouse-anti-transferrin receptor monoclonal antibody (PE-mAb-Tfr) was conjugated to the surface of drug loaded PLGA nanoparticles by the two-step carbodiimide process, which involved the activation of the carboxyl groups on the nanoparticle surface by an EDC/NHS mixture, followed by binding of the activated carboxyl groups to the amino groups in the antibody (Weissenbfck et al 2004). The effect of EDC-HCl concentration, pH, temperature, reaction time and antibody (PE-mAb-Tfr) to nanoparticles (NPs) ratio on conjugation efficiency and particle size was also studied.

Briefly in first step, to the lyophilized drug containing nanoparticles dispersed in phosphate buffer pH adjusted to 5.0, using potassium dihydrogen phosphate, was

added freshly prepared aqueous solution of EDC-HCl with continuos stirring on a magnetic stirrer followed by an equimolar freshly prepared aqueous solution of NHS after half an hour. Then, the mixture was allowed to stir on a magnetic stirrer for 30 mins more. Then the activated nanoparticles were recovered by centrifuging at 10000 rpm for 15 min, washed with distilled water and suspended in phosphate buffer pH 7.4 (pH adjusted if required).The temperature was maintained below 15°C throughout the conjugation using ice-bath.

In the second step, to the dispersion of activated nanoparticles was added solution of PE-mAb-Tfr in phosphate buffer pH 7.4. The mixture was stirred for one hour, centrifuged at 13000 rpm for 15 mins at 15°C to separate PE-mAb-Tfr conjugated nanoparticles and washed twice with phosphate-buffered saline (PBS) 7.4 to remove unreacted reagents and PE-mAb-Tfr. The temperature was maintained below 15°C throughout the conjugation using ice-bath. To saturate the free coupling sites 1.0 ml of 20 % glycine solution in 20mM HEPES/NaOH buffer, pH 7.4 was added and incubated for 1 hr. Finally, the particles were washed with distil water and lyophilized for 24hrs

Estimation of conjugation efficiency of antibody to the nanoparticles

The amount of PE-mAb-Tfr conjugated to the nanoparticles was estimated spectrofluorometrically at an excitation and emission wavelengths of 488nm and 578 nm respectively against PBS 7.4 as blank. The amount of the unconjugated PE-mAb-Tfr in the supernant and the washings was subtracted from the amount of the PE-mAb-Tfr added for conjugation. The % conjugation efficiency was calculated as follows:

$$\%CE = \frac{(PE-mAb-Tfr\ added\ for\ conjugation) - (PE-mAb-Tfr\ unconjugated)}{(PE-mAb-Tfr\ added\ for\ conjugation)} * 100$$

Influence of pH on conjugation efficiency

The effect of pH on the conjugation efficiency of PE-mAb-Tfr to nanoparticles was checked by varying the pH during activation, i.e. step 1, between 5 to7 keeping pH during antibody conjugation, i.e. step 2, at 7.4 to avoid any protein denaturation. The weight of PE-mAb-Tfr to weight of nanoparticles ratio was taken as 1:10,

concentration of EDC-HCl and NHS as 7 μM, activation time as 1 hr (step 1) and reaction temperature as 15°C and the results are recorded in table 4.17.

Influence of temperature on conjugation efficiency

The effect of temperature on PE-mAb-Tfr conjugation to nanoparticles was tested by varying the reaction temperature (of step 1 and step 2) between 15-45°C and the results are recorded in table 4.18. The weight of PE-mAb-Tfr to weight of nanoparticles ratio was taken as 1:10, concentration of EDC-HCl and NHS as 7 μM, activation time as 1 hr (step 1) and activation pH as 5 for step 1 and 7.4 for step 2.

Influence of amount of activating agent [EDC-HCl/NHS concentration]

The influence of the amount of activating agent (EDC-HCl/NHS concentration) on conjugation efficiency of PE-mAb-Tfr to nanoparticles was assessed by varying the amount of EDC-HCl/NHS, keeping the weight of PE-mAb-Tfr to weight of nanoparticles ratio as 1:10, pH as 5 during activation and 7.4 during conjugation, activation time as 1 hr (step 1) and reaction temperature as 15°C and the results are recorded in table 4.19.

Influence of reaction time

The influence of reaction time (activation and conjugation time i.e. time for step 1 + step 2) on conjugation efficiency of PE-mAb-Tfr to nanoparticles was assessed by varying the PLGA nanoparticles activation time, keeping the weight of PE-mAb-Tfr to weight of nanoparticles ratio as 1:10; pH as 5 during activation and 7.4 during conjugation, concentration of EDC-HCl and NHS as 7.8 μM and reaction temperature as 15°C and the results are recorded in table 4.20.

Influence of amount of antibody

The effect of amount of antibody (PE-mAb-Tfr) on conjugation efficiency and particle size was checked by varying the amount of antibody added to the activated nanoparticles. The concentration of EDC-HCl and NHS was taken as 7 μM, activation pH as 5 for step 1 and 7.4 for step 2 and reaction temperature as 15°C and the results are recorded in table 4.21.

4.1.2 Characterization of nanoparticles

4.1.2.1 [^{1}H]NMR of the antibody conjugated nanoparticles

^{1}H-NMR spectroscopy was used to ascertain the conjugation of PE-mAb-Tfr to the nanoparticles. The ^{1}H-NMR spectra of NNp and PE-mAb-Tfr-NNp are shown in figure 4.8.

4.2.2 Particle size and zeta potential

A 2.0 mg sample of lyophilized drug containing nanoparticles, unconjugated and antibody conjugated, was suspended in distilled water, and the particle size and zeta potential were measured using the principle of laser light scattering with zeta sizer (Nano-ZS, Malvern Instruments, UK). The observations are tabulated in table 4.22 and figures 4.9 to 4.14 for the nanoparticles of the three drugs.

4.1.2.3 Drug entrapment efficiency

To determine the amount of NG, SB and HG entrapped in the NPs, 2mg of NPs were added to 2 ml of acetonitrile and subjected to shaking at room temperature for 4hrs for complete dissolution of PLGA for extraction of drug from the nanoparticles. The resulting system was centrifuged at 5000rpm for 15mins to remove the precipitated components. The supernant was further diluted suitably with acetonitrile and estimated using 2nd derivative UV spectrophotometry at 320 nm, 282.2 nm and 298.5 nm for NG, SB and HG respectively. The % drug entrapment efficiency (EE) was calculated using the following equation and the results are recorded in table 4.22.

$$\% EE = \frac{amount\ of\ drug\ in\ nanoparticles}{Drug\ added\ in\ formulation} * 100$$

4.1.2.4 In-vitro drug release

The invitro drug release of the nanoparticles of temozolomide was performed in phosphate-buffer saline (PBS) pH 7.4 at 37°C (Shen Gao et al 2007). The release study for NG nanoparticles was performed in 10 % methanolic phosphate buffer saline pH 7.4 + 2 %w/w polysorbate-80, while for HG and SB in 10 % methanolic phosphate buffer saline pH 7.4 + 2 %w/w polysorbate-80 and 30 % ethanolic phosphate buffer saline pH 7.4 + 2 %w/w polysorbate-80 respectively (Jagdish Singh, 2000). Nanoparticles equivalent to 1mg drug were suspended in 10 ml of release media in screw capped tubes, which were placed in horizontal shaker bath maintained

123

at 37°C and shaken at 60 rpm. At specific time intervals following incubation samples were taken out and centrifuged at 15000rpm for 30min. The residue was collected and dissolved in acetonitrile, diluted suitably and analyzed by UV spectrophotometer for respective drug. The amount of the drug released was calculated using the following equation. The release of drug from the unconjugated and conjugated nanoparticles is tabulated in table 4.23 and shown graphically in figure 4.15 for NG, SB and HG respectively.

$$\% \text{ Drug released} = \left[1 - \left(\frac{\text{Amount of drug in nanoparticles settled}}{\text{Amount of drug initially present in nanoparticles}} \right) \right] \times 100$$

4.1.2.5 Transmission electron microscopy

Nanoparticles were dispersed in de-ionized water at a concentration of 1mg/ml. To measure the morphology and size distribution of nanoparticles, a drop of sample was placed onto a 300-mesh copper grid coated with carbon. Approximately 2 min after deposition, the grid was tapped with filter paper to remove surface water and air-dried. Negative staining was performed using a droplet of 0.5% w/v phosphotungstic acid. Transmisssion electron microscopy was performed using Morgagni 268, Philips (Netherlands) transmission electron microscope. The TEM images for unconjugated and antibody conjugated nanoparticles of NG, HG and SB are shown in figures 4.16, 4.17 and 4.18 respectively.

4.1.2.6 Differential Scanning Calorimetry

DSC of the drugs, PLGA and drug containing nanoparticles were performed using differential scanning calorimetry instrument. Thermograms were analyzed using Mettler Toledo star SW 7.01/8.10. An empty aluminium pan was used as the reference for all measurements. During each scan, 3-5 mg of sample was heated, in a hermetically sealed aluminium pan, at a heating rate of 10° C/min, from 35-50° C to 300° C, under a nitrogen atmosphere. Figure 4.19 A, B and C show the thermograms for PLGA, NG and NNp. Similarly, Figure 4.20 A, B and C show the thermograms for PLGA, HG and HNp and figure 4.21 A, B, C and D show the thermograms for PLGA, SBMH, SB and SNp.

4.1.2.7 *Stability studies*

The stability studies were carried out in accordance with the ICH guidelines for new drug products. The stability studies were carried out for the nanoparticle formulations at 5°C ± 3°C for 6 months and (25°C±2°C/60±5% RH) up to 6 months. Three batches at optimized process and formulation conditions were prepared and subjected to stability studies. The nanoparticles were filled in glass vials, closed with rubber closures and sealed with aluminium caps. The samples were withdrawn at predetermined time and were examined visually for physical appearance. The contents of the vials were evaluated for the particle size, zeta potential and drug content. The data were compared using ANOVA and student's t-test and difference larger than the value at p<0.05 were considered significant. The results of stability studies for NG, HG and SB nanoparticles are tabulated in tables 4.24, 4.25 and 4.26 respectively.

4.1.2.8 *Determination of residual dichloromethane/chloroform in nanoparticles*

As per USP, residual solvents are tested under General Chapter <467> "Organic Volatile Impurities." Dichloromethane and chloroform belongs to class 2 solvents. Class 2 solvents are non-genotoxic animal carcinogens. Solvents of this class should be limited in pharmaceutical products because of their inherent toxicity. Limit for dichloromethane is 600ppm with permissible daily exposure of 6 mg/day and for chloroform is 60ppm with permissible daily exposure of 0.6 mg/day. Dichloromethane and chloroform were analyzed for NG and HG containing unconjugated and antibody conjugated nanoparticles respectively by gas chromatography coupled with static headspace sampling, the operating parameters of which are listed in table 4.2.

Table 4.2 Headspace operating parameters

	Headspace operating parameter sets		
	1	2	3
Equilibration temperature °C	80	105	80
Equilibration time (min.)	60	45	45
Transfer-line temperature °C	85	110	105
Carrier gas: nitrogen or helium at an appropriate pressure			
Pressurization time (s)	30	30	30
Injection volume (mL)	1	1	1

4.2 Results

4.2.1 Precipitation of sibutramine base (SB) from Sibutramine hydrochloride monohydrate (SBHM) salt

The yield of SB from SBHM was found to be 85±5% and the melting point was observed to be 50°±1°C. The DSC thermograms of SBHM and SB are shown in figure 5.7.

4.2.2 Preparation and optimization of nanoparticles

The emulsion solvent evaporation method is one of the most frequently used methods yielding spherical nanoparticles with smooth surfaces (Nagesh Bandi, 2004) and hence was used to prepare nanoparticles in this investigation.

Table 4.3: Optimization of rate of addition of organic phase

Sr. No.	Rate of organic phase addition (mL/min)	Particle size (nm)	Entrapment efficiency (%w/w)
1	0.5	250 ± 36	83.2 ± 3.3
2	1.5	169 ± 25	79.5 ± 4.1
3	2.5	210 ± 40	84.1 ± 3.5

(Values are Mean ± S.D., $n = 3$)

Table 4.4: Influence of stirring speed

Sr. No.	Stirrer speed (rpm)	Particle size (nm)	Entrapment efficiency (%w/w)
1	900	253 ± 36	83.2 ± 4.3
2	1200	178 ± 25 nm	80.9 ± 3.2
3	1500	160.4 ± 40 nm	71.9 ± 3.9

(Values are Mean ± S.D., $n = 3$)

Table 4.5: Optimization of probe sonication time

Sr. No.	Sonication time (sec)	Particle size (nm)	Entrapment efficiency (%w/w)
1	60	201 ± 28	81.5 ± 3.3
2	90	172 ± 32	79.5 ± 2.6
3	120	161 ± 35	69.7 ± 4.9

(Values are Mean ± S.D., $n = 3$)

Table 4.6: Influence of stirring time

Sr. No.	Stirring time (min)	Particle size (nm)	Entrapment efficiency (%w/w)
1	15	213 ± 24	82.2 ± 2.3
2	30	178 ± 29 nm	79.9 ± 3.1
3	45	209 ± 26 nm	70.9 ± 2.7

(Values are Mean ± S.D., $n = 3$)

Table 4.7: 3^3 factorial experimental design for NG nanoparticles

Batch No.	X_1	X_2	X_3	NNp PS (nm)	NNp %EE
1	-1	-1	-1	250.2	78.3
2	0	-1	-1	210.6	75.8
3	1	-1	-1	187.1	70.2
4	-1	0	-1	201.2	78.4
5	0	0	-1	169.2	75.2
6	1	0	-1	128.5	70.6
7	-1	1	-1	201.2	74.7
8	0	1	-1	156.7	72.1
9	1	1	-1	124.3	68.3
10	-1	-1	0	274.2	83.7
11	0	-1	0	248.6	82.9
12	1	-1	0	213.7	78.4
13	-1	0	0	228.9	83.6
14	0	0	0	173.6	81.2
15	1	0	0	136.3	74.5
16	-1	1	0	203.7	77.9
17	0	1	0	159.5	75.1
18	1	1	0	131.3	69.4
19	-1	-1	1	298.5	84.8
20	0	-1	1	271.4	83.1
21	1	-1	1	239.6	79.7
22	-1	0	1	273.1	85.4
23	0	0	1	241.8	84.1
24	1	0	1	230.6	82.9
25	-1	1	1	258.3	81.7
26	0	1	1	231.7	78.5
27	1	1	1	211.8	73.2

Table 4.8: 3^3 factorial experimental design for HG nanoparticles

Batch No.	X_1	X_2	X_3	HNp PS (nm)	HNp %EE
1	-1	-1	-1	267.1	62.9
2	0	-1	-1	250.8	61.3
3	1	-1	-1	237.4	58.6
4	-1	0	-1	217.2	57.9
5	0	0	-1	191.3	54.1
6	1	0	-1	169.5	50.4
7	-1	1	-1	197.6	55.9
8	0	1	-1	170.3	52.1
9	1	1	-1	159.7	48.3

10	-1	-1	0	289.1	69.2
11	0	-1	0	271.2	68.7
12	1	-1	0	258.6	68.1
13	-1	0	0	235.2	67.3
14	0	0	0	198.6	65.8
15	1	0	0	174.9	59.4
16	-1	1	0	231.2	60.7
17	0	1	0	192.1	56.6
18	1	1	0	176.3	51.9
19	-1	-1	1	301.6	69.7
20	0	-1	1	284.2	65.3
21	1	-1	1	266.1	61.6
22	-1	0	1	253.8	68.4
23	0	0	1	230.4	66.1
24	1	0	1	207.3	60.9
25	-1	1	1	271.5	59.2
26	0	1	1	257.2	54.8
27	1	1	1	233.8	53.2

Table 4.9: 3^3 factorial experimental design for SB nanoparticles

Batch No.	X_1	X_2	X_3	SNp	
				PS (nm)	%EE
1	-1	-1	-1	285.2	64.8
2	0	-1	-1	261.9	62.4
3	1	-1	-1	239.6	60.1
4	-1	0	-1	223.4	57.9
5	0	0	-1	205.1	56.3
6	1	0	-1	187.5	54.8
7	-1	1	-1	179.8	52.2
8	0	1	-1	161.4	50.7
9	1	1	-1	138.6	49.3
10	-1	-1	0	301.6	67.4
11	0	-1	0	287.2	66.5
12	1	-1	0	261.7	65.1
13	-1	0	0	249.5	63.8
14	0	0	0	210.3	62.5
15	1	0	0	194.1	59.1
16	-1	1	0	187.4	56.3
17	0	1	0	174.7	53.6
18	1	1	0	145.5	52.1
19	-1	-1	1	310.1	68.8
20	0	-1	1	295.6	67.2
21	1	-1	1	272.3	65.9
22	-1	0	1	264.7	64.6

23	0	0	1	241.2	63.9
24	1	0	1	231.4	59.9
25	-1	1	1	215.1	57.5
26	0	1	1	193.2	55.1
27	1	1	1	175.6	53.6

Table 4.10: Analysis of variance of full and reduced model for NNp

		Df	SS	MS	F	R	R^2	Adj R^2
Regression (PS)	FM	10	58472.35	5847.235	31.20978	0.976802	0.954142	0.92357
	RM	5	57763.54	11552.71	65.65716	0.970863	0.942576	0.92822
Error (PS)	FM	15	2810.29 (E1)	187.3527				
	RM	20	3519.101 (E2)	175.955				
Regression (%EE)	FM	10	656.6099	65.66099	30.44553	0.97624	0.953045	0.921742
	RM	4	633.686	158.4215	60.18835	0.959047	0.919772	0.90449
Error (%EE)	FM	15	32.35006 (E1)	2.156671				
	RM	21	55.27401 (E2)	2.632096				

Number of parameters omitted = 5 (PS); 6 (%EE).

†SSE2 − SSE1 = 3519.101-2810.29=708.811 (PS); 55.27401-32.35006=22.92395 (%EE)

‡MS of error (full model) = 187.3527 (PS); 2.156671 (%EE)

§F calculated = (708.811/5)/187.3527= 0.7566 (PS); (22.92395/6)/2.156671=1.772 (%EE)

F tabulated (5) = 2.571; F tabulated (6) = 2.447

Since F cal < F tab, the omitted parameter is non significant and the hypothesis is accepted

Table 4.11: Analysis of variance of full and reduced model for HNp

		Df	SS	MS	F	R	R^2	Adj R^2
Regression (PS)	FM	10	44699.32	4469.932	31.8675	0.977265	0.955046	0.925077
	RM	5	44264.74	8852.947	69.74741	0.972502	0.945761	0.932201
Error (PS)	FM	15	2103.993 (E1)	140.2662				
	RM	20	2538.574 (E2)	126.9287				
Regression (%EE)	FM	10	1007.036	100.7036	21.2199	0.966426	0.933979	0.889964
	RM	4	978.8675	244.7169	51.72468	0.952814	0.907854	0.890302
Error (%EE)	FM	15	71.18572 (E1)	4.745714				
	RM	21	99.35401 (E2)	4.731143				

Number of parameters omitted = 5 (PS); 6 (%EE).

†SSE2 – SSE1 = 2538.574-2103.993=434.581 (PS); 99.35401-71.18572=28.16829 (%EE)

‡MS of error (full model) = 140.2662 (PS); 4.745714 (%EE)

§F calculated = (434.581/5)/140.2662= 0.6196 (PS); (28.16829/6)/4.745714=0.989 (%EE)

F tabulated (5) = 2.571; F tabulated (6) = 2.447

Since F cal < F tab, the omitted parameter is non significant and the hypothesis is accepted

Table 4.12: Analysis of variance of full and reduced model for SNp

		Df	SS	MS	F	R	R^2	Adj R^2
Regression (PS)	FM	10	64891.02	6489.102	73.24036	0.989914	0.979931	0.966551
	RM	4	68715.14	17178.78	261.9042	0.989663	0.979432	0.975692
Error (PS)	FM	15	1329.001 (E1)	88.60009				
	RM	22	1443.021 (E2)	65.59187				
Regression (%EE)	FM	10	830.6825	83.06825	148.1352	0.994975	0.989976	0.983293
	RM	4	813.8067	203.4517	168.9588	0.984817	0.969864	0.964124
Error (%EE)	FM	15	8.411396 (E1)	0.56076				
	RM	21	25.28714 (E2)	1.20415				

Number of parameters omitted = 4 (PS); 4 (%EE).

†SSE2 – SSE1 = 1443.021-1329.001=114.02 (PS); 25.28714-8.411396=16.875744 (%EE)

‡MS of error (full model) = 88.60009 (PS); 0.56076 (%EE)

§F calculated = (114.02/4)/ 88.60009= 0.7566 (PS); (16.875744/6)/ 0.56076=2.316 (%EE)

F tabulated (4) = 2.571; F tabulated (6) = 2.447

Since F cal < F tab, the omitted parameter is non significant and the hypothesis is accepted

Figure 4.2: Contour plot for particle size of NNp

Contours of PS at -1 level of X3

C3
— 120.0
134.0
148.0
162.0
176.0
190.0
204.0
218.0
232.0
246.0

(a) -1 level of X3

Contours of PS at 0 level of X3

(b) 0 level of X3

Contours of PS at 1 level of X3
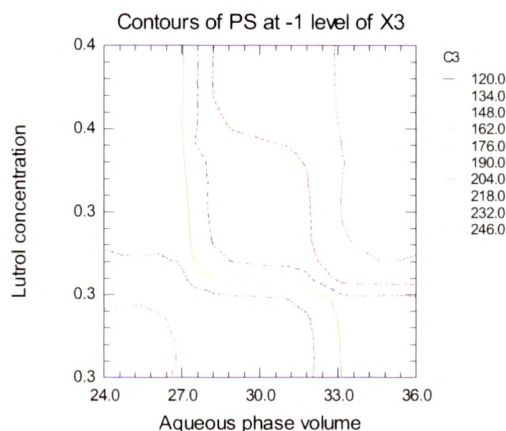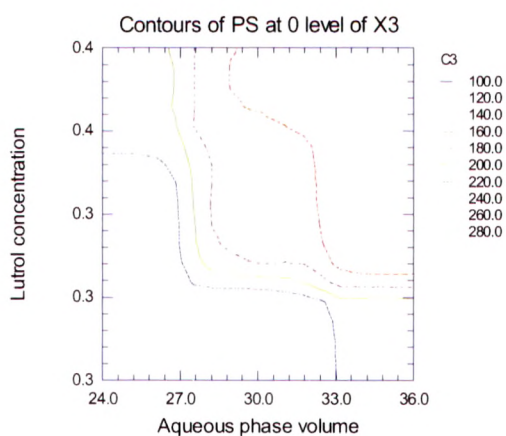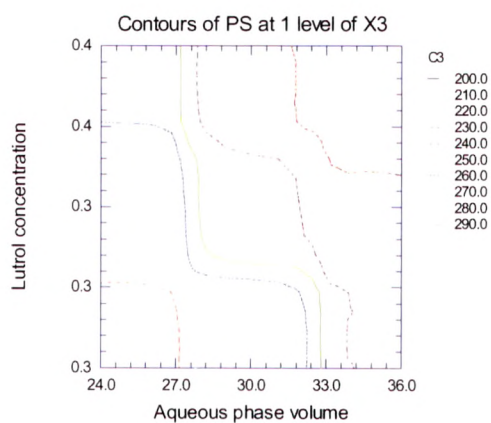
(c) 1 level of X3

Figure 4.3: Contour plot for percentage drug entrapment efficiency of NNp

Contours of %EE at -1 level of X3


(a) -1 level of X3

131
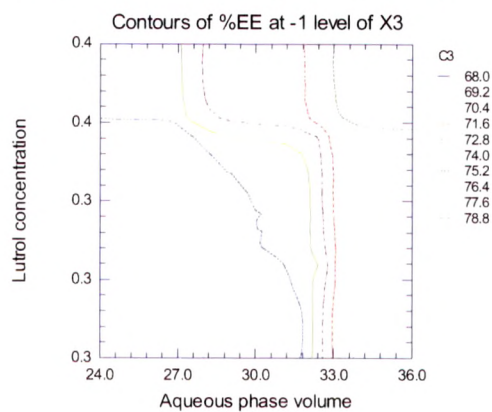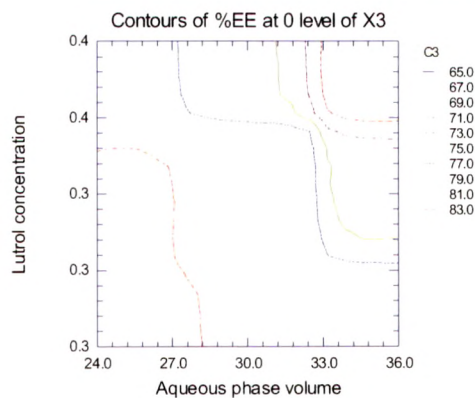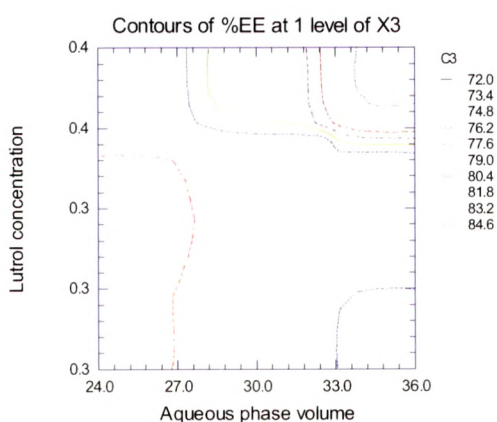
(b) 0 level of X3

(c) 1 level of X3

**Figure 4.4: Contour plot for particle size of HNp**


(a) -1 level of X3

Contours of PS at 0 level of X3

C3
160.0
174.0
188.0
202.0
216.0
230.0
244.0
258.0
272.0
286.0

Lutrol concentration

Aqueous phase volume

(b) 0 level of X3

Contours of PS at 1 level of X3

C3
200.0
212.0
224.0
236.0
248.0
260.0
272.0
284.0
296.0
308.0

Lutrol concentration

Aqueous phase volume
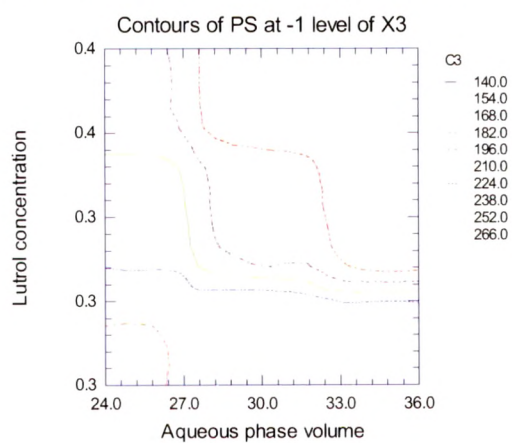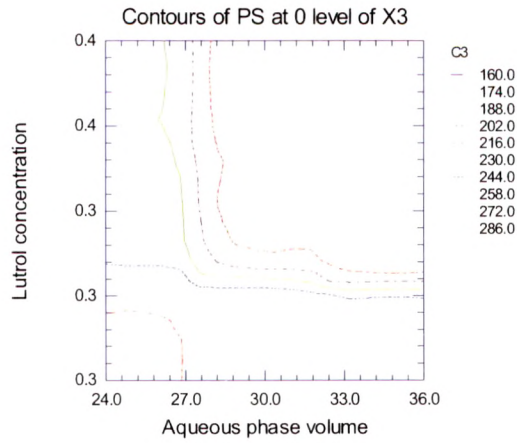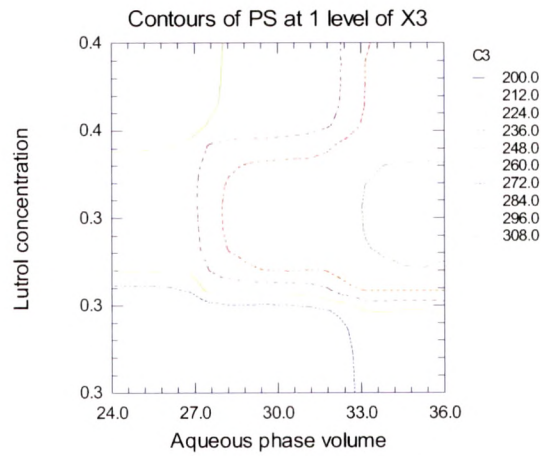
(c) 1 level of X3

Figure 4.5: Contour plot for percentage drug entrapment efficiency of HNp

Contours of %EE at -1 level of X3

C3
45.0
47.0
49.0
51.0
53.0
55.0
57.0
59.0
61.0
63.0

Lutrol concentration

Aqueous phase volume

(a) -1 level of X3

133

Contours of %EE at 0 level of X3

(b) 0 level of X3

Contours of %EE at 1 level of X3
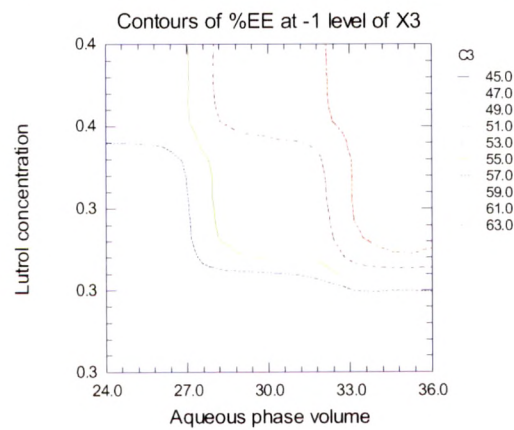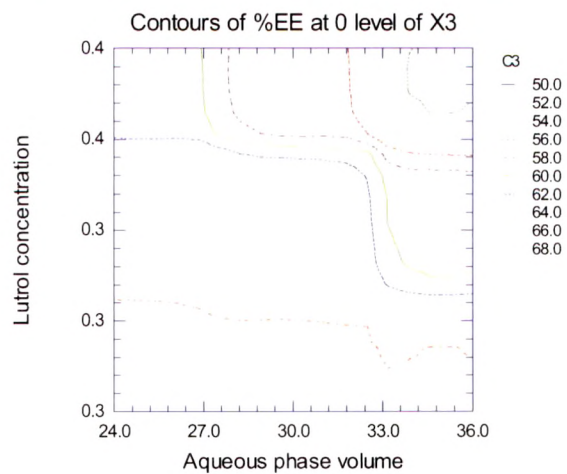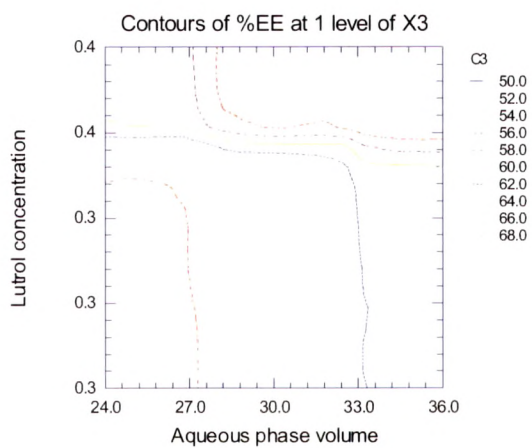
(c) 1 level of X3

Figure 4.6: Contour plot for particle size of SNp

Contours of PS at -1 level of X3

(a) -1 level of X3

Contours of PS at 0 level of X3

(b) 0 level of X3

Contours of PS at 1 level of X3
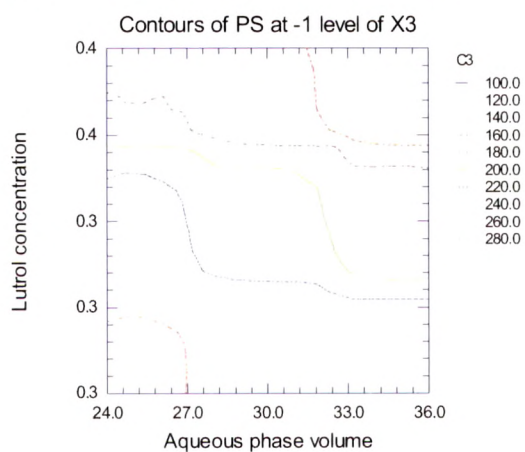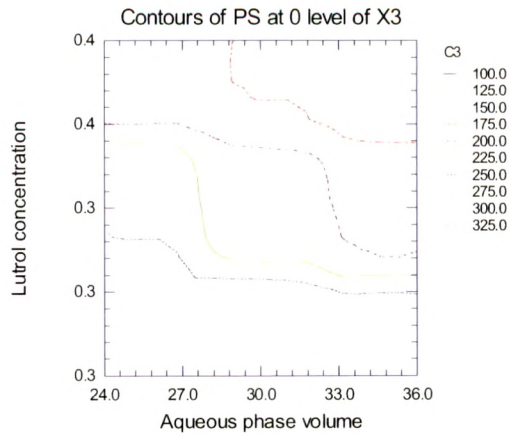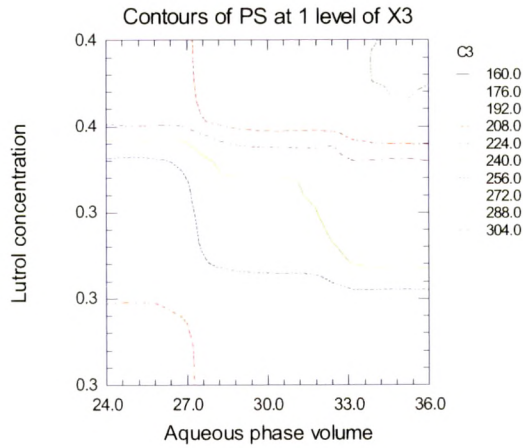
(c) 1 level of X3

Figure 4.7: Contour plot for percentage drug entrapment efficiency of SNp

Contours of %EE at -1 level of X3
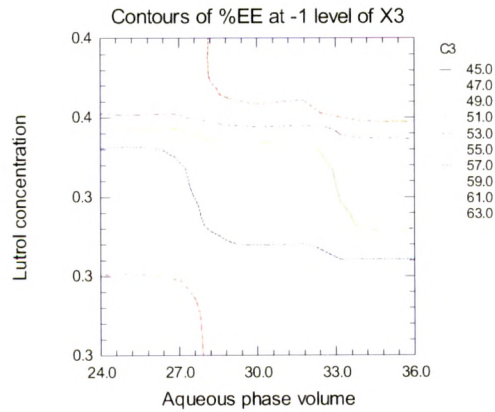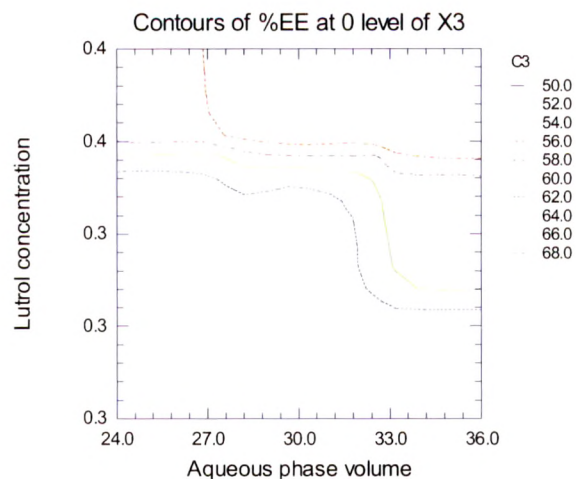
(a) -1 level of X3
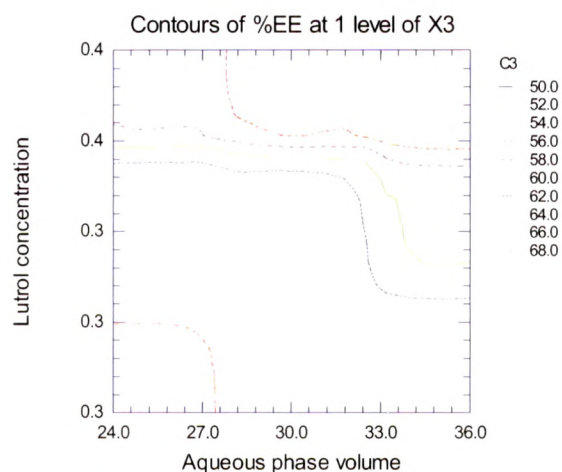
(b) 0 level of X3

(c) 1 level of X3

Table 4.13: Check point analysis for NNp

No.		Values from contours		Particle size (nm)		Percentage entrapment efficiency (%w/w)	
	X3	X1	X2	Predicted	Experimental**	Predicted	Experimental**
1	-1	30.35294	0.274118	210.5877	208.4±1.72	75.79886	73.5±1.24
2	0	28.94118	0.274118	248.5197	247.1±1.24	82.89965	81.9±1.76
3	1	32.47059	0.274118	255.8363	257.7±2.11	81.54902	80.4±2.03

*Difference between predicted and experimental values were found to be insignificant (P>0.05)

** n = 3

Table 4.14: Check point analysis for particle size for HNp

No.		Values from contours		Particle size (nm)		Percentage entrapment efficiency (%w/w)	
	X3	X1	X2	Predicted	Experimental**	Predicted	Experimental**
1	-1	26.11765	0.267059	266.8719	268.2 ±1.94	62.8774	60.7±1.37
2	0	29.64706	0.267059	271.1976	269.7±2.08	68.69988	67.8±1.82
3	1	32.47059	0.267059	274.8056	275.6±1.47	63.57919	62.3±1.19

*Difference between predicted and experimental values were found to be insignificant (P>0.05)
** n = 3

Table 4.15: Check point analysis for particle size for SNp

No.		Values from contours		Particle size (nm)		Percentage entrapment efficiency (%w/w)	
	X3	X1	X_2	Predicted	Experimental**	Predicted	Experimental**
1	-1	25.41176	0.302353	228.3849	223.7 ±1.62	58.46392	56.2±1.71
2	0	30.35294	0.302353	216.3686	214.6±1.39	62.78415	61.5±1.48
3	1	27.52941	0.302353	258.5012	257.2±1.85	64.6465	63.9±1.54

*Difference between predicted and experimental values were found to be insignificant (P>0.05)
** n = 3

4.2.3 Lyophilization and optimization of cryoprotectant concentration:

Table 4.16: Effect of different cryoprotectants on the particle size and redispersion of NG nanoparticles

Type of cryoprotectant	NP: CP	Particle size (nm)		S_f/S_i	Redispersion
		Before lyophilization S_i	After lyophilization S_f		
Initial	1:0	181 ± 9	NA	NA	NA
Sucrose	1:2	--	589 ± 8	3.25	Poor redispersibility
Sucrose	1:3	--	458 ± 11	2.53	Poor redispersibility
Sucrose	1:4	--	410 ± 7	2.27	Poor redispersibility
Mannitol	1:2	--	419 ± 9	2.32	Difficult redispersibility
Mannitol	1:3	--	368 ±10	2.03	Difficult redispersibility
Mannitol	1:4	--	313 ± 8	1.18	Difficult redispersibility
Trehalose	1:2	--	307 ± 7	1.7	Difficult redispersibility
Trehalose	1:3	--	246 ± 8	1.36	Easy redispersibility
Trehalose	**1:4**	--	**195 ± 9**	**1.08**	**Easy redispersibility**

(Values are Mean ± S.D., *n* = 3)
NA: Not Applicable

4.2.4 Antibody conjugation of nanoparticles:

Table 4.17: Optimization of antibody conjugation activation pH

pH	Conjugation efficiency (%w/w)			Mean particle size (nm)			%EE (%w/w)		
	PE-mAb-Tfr-NNp	PE-mAb-Tfr-SNp	PE-mAb-Tfr-HNp	PE-mAb-Tfr-NNp	PE-mAb-Tfr-SNp	PE-mAb-Tfr-HNp	PE-mAb-Tfr-NNp	PE-mAb-Tfr-SNp	PE-mAb-Tfr-HNp
4	30.3 ± 1.9	28.9 ± 3.4	27.3 ± 2.1	202.1 ± 5.1	219.3 ± 5.7	210.5 ± 6.6	69.5 ± 2.1	46.7 ± 1.6	49.3 ± 1.9
5	35.3 ± 1.9	33.9 ± 3.4	34.4 ± 2.4	199.4 ± 6.2	218.9 ± 4.9	213.2 ± 8.1	74.3 ± 1.4	59.4 ± 1.4	60.7 ± 1.2
6	23.5 ± 2.6	25.9 ± 3.1	22.4 ± 2.8	201.8 ± 4.9	221.3 ± 3.8	211.6 ± 5.2	77.4 ± 1.9	61.1 ± 1.2	63.9 ± 1.7
7	16.1 ± 3.1	14.4 ± 2.2	15.7 ± 2.6	197.5 ± 5.5	219.8 ± 7.1	211.6 ± 5.2	78.9 ± 2.2	61.9 ± 2.1	61.8 ± 2.3

(Values are Mean ± S.D., n = 3)

Table 4.18: Optimization of antibody conjugation reaction temperature

Temperature (°C)	Conjugation efficiency (%w/w)			Mean particle size (nm)			%EE (%w/w)		
	PE-mAb-Tfr-NNp	PE-mAb-Tfr-SNp	PE-mAb-Tfr-HNp	PE-mAb-Tfr-NNp	PE-mAb-Tfr-SNp	PE-mAb-Tfr-HNp	PE-mAb-Tfr-NNp	PE-mAb-Tfr-SNp	PE-mAb-Tfr-HNp
15	33.2 ± 2.9	34.9 ± 1.6	31.4 ± 3.1	200.2 ± 5.1	225.7 ± 4.3	211.4 ± 4.7	79.3 ± 1.6	61.4 ± 1.3	63.7 ± 1.4
30	23.4 ± 1.9	24.2 ± 2.6	25.2 ± 2.1	195.2 ± 5.8	222.7 ± 4.9	208.3 ± 5.9	70.5 ± 2.2	52.7 ± 2.3	54.3 ± 2.4
45	16.9 ± 2.4	15.4 ± 3.2	17.7 ± 2.9	182.9 ± 3.7	211.4 ± 4.2	199.3 ± 4.6	59.1 ± 1.3	39.1 ± 1.8	38.7 ± 1.8

(Values are Mean ± S.D., n = 3)

Table 4.19: Optimization of amount of activating agent

Amount of EDC-HCl/NHS (µM)	Conjugation efficiency (%w/w)			Mean particle size (nm)			%EE (%w/w)		
	PE-mAb-Tfr-NNp	PE-mAb-Tfr-SNp	PE-mAb-Tfr-HNp	PE-mAb-Tfr-NNp	PE-mAb-Tfr-SNp	PE-mAb-Tfr-HNp	PE-mAb-Tfr-NNp	PE-mAb-Tfr-SNp	PE-mAb-Tfr-HNp
7.3	31.2 ± 2.9	29.9 ± 1.6	30.4 ± 3.1	196.2 ± 6.2	227.6 ± 4.9	209.8 ± 6.6	78.3 ± 2.6	62.4 ± 2.1	63.3 ± 2.6
7.8	39.5 ± 2.9	40.5 ± 1.6	38.9 ± 2.2	201.6 ± 7.4	220.4 ± 5.7	213.2 ± 8.1	77.1 ± 1.7	61.7 ± 1.6	62.8 ± 2.1
8.3	40.9 ± 2.3	38.7 ± 2.2	39.8 ± 1.9	198.8 ± 5.8	219.6 ± 2.2	211.6 ± 5.2	79.8 ± 2.3	63.7 ± 1.2	64.1 ± 1.9

(Values are Mean ± S.D., n = 3)

Table 4.20: Optimization of antibody conjugation reaction time

Reaction time (hr)	Conjugation efficiency (%w/w)			Mean particle size (nm)			%EE (%w/w)		
	PE-mAb-Tfr-NNp	PE-mAb-Tfr-SNp	PE-mAb-Tfr-HNp	PE-mAb-Tfr-NNp	PE-mAb-Tfr-SNp	PE-mAb-Tfr-HNp	PE-mAb-Tfr-NNp	PE-mAb-Tfr-SNp	PE-mAb-Tfr-HNp
1	29.2 ± 1.8	28.5 ± 2.1	28.8 ± 1.7	192.2 ± 4.2	222.5 ± 5.9	203.4 ± 4.6	79.1 ± 1.7	63.1 ± 1.8	62.9 ± 1.6
2	39.4 ± 1.5	39.1 ± 1.9	39.7 ± 1.5	203.6 ± 5.6	217.3 ± 4.7	210.6 ± 5.1	78.4 ± 2.3	62.5 ± 1.3	61.6 ± 1.8
3	40.9 ± 2.1	39.7 ± 1.6	39.2 ± 2.1	194.8 ± 3.8	214.7 ± 4.2	207.3 ± 3.2	75.5 ± 1.9	59.7 ± 1.6	58.2 ± 2.1

(Values are Mean ± S.D., n = 3)

Table 4.21: Optimization of amount of antibody

Antibody amount (Antibody:NPs ratio)	Conjugation efficiency (%w/w)			Mean particle size (nm)			%EE (%w/w)		
	PE-mAb-Tfr-NNp	PE-mAb-Tfr-SNp	PE-mAb-Tfr-HNp	PE-mAb-Tfr-NNp	PE-mAb-Tfr-SNp	PE-mAb-Tfr-HNp	PE-mAb-Tfr-NNp	PE-mAb-Tfr-SNp	PE-mAb-Tfr-HNp
500 µg (1:1)	43.5 ± 1.2	44.1 ± 1.1	42.6 ± 1.4	189.7 ± 6.4	231.1 ± 5.8	209.8 ± 6.7	78.6 ± 1.6	62.9 ± 1.8	62.8 ± 2.6

			39.7 ± 3.2	197.3 ± 5.9	233.6 ± 5.6	215.1 ± 5.6	77.9 ± 2.3	62.5 ± 1.4	63.2 ± 2.
20 µg (1:25)	39.1 ± 2.5	38.8 ± 2.7							
10 µg (1:50)	20.5 ± 2.6	21.4 ± 3.2	19.9 ± 2.2	194.8 ± 6.7	228.2 ± 7.1	211.5 ± 5.8	78.9 ± 1.5	63.3 ± 2.1	63.6 ± 1.

(Values are Mean ± S.D., *n* = 3)

4.2.5 Characterization of nanoparticles:

Figure 4.8: ^{1}H-NMR of [A] NNp [B] PE-mAb-Tfr-NNp

A   B
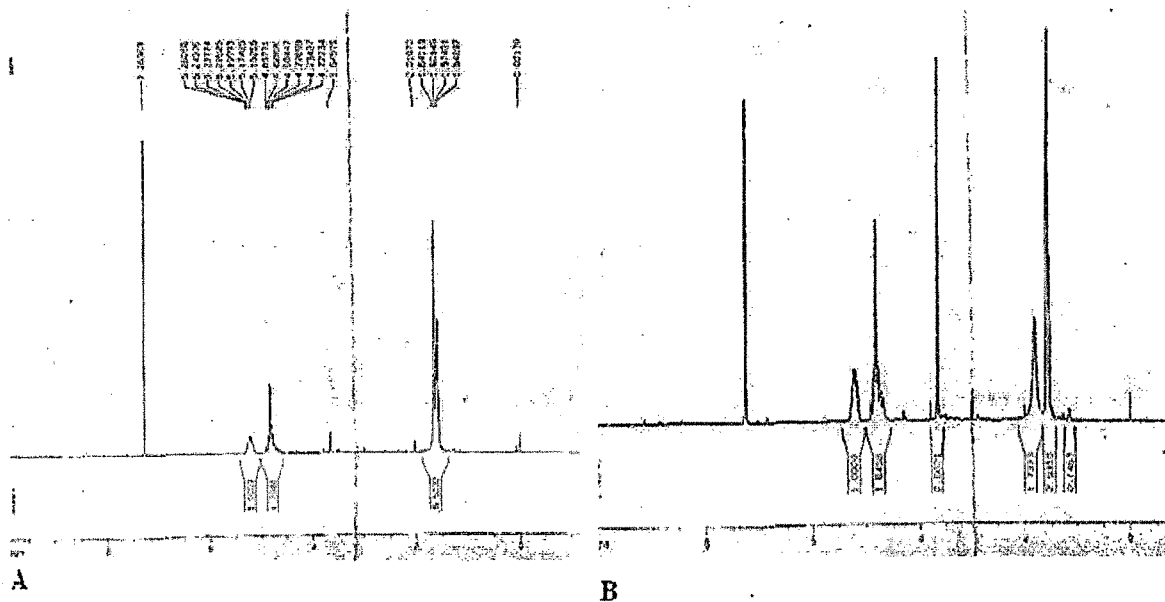
Table 4.22: Characterization of optimized drug containing nanoparticles

Formulation	Mean PS (nm)	%EE (%w/w)	Antibody conjugation efficiency (%w/w)
NNp	173.6 ± 6.1	81.2 ± 2.1	----
SNp	210.3 ± 5.7	62.5 ± 1.5	----
HNp	198.6 ± 5.3	65.8 ± 1.3	----
PE-mAb-Tfr-NNp	195.7 ± 6.4	77.9 ± 1.5	43.5 ± 1.2
PE-mAb-Tfr-SNp	230.4 ± 6.7	60.6 ± 1.8	42.6 ± 1.4
PE-mAb-Tfr-HNp	221.3 ± 5.8	63.4 ± 2.1	44.1 ± 1.1

(Values are Mean ± S.D., *n* = 3)

Figure 4.9: Particle size distribution plot of nicergoline nanoparticles before and after antibody conjugation
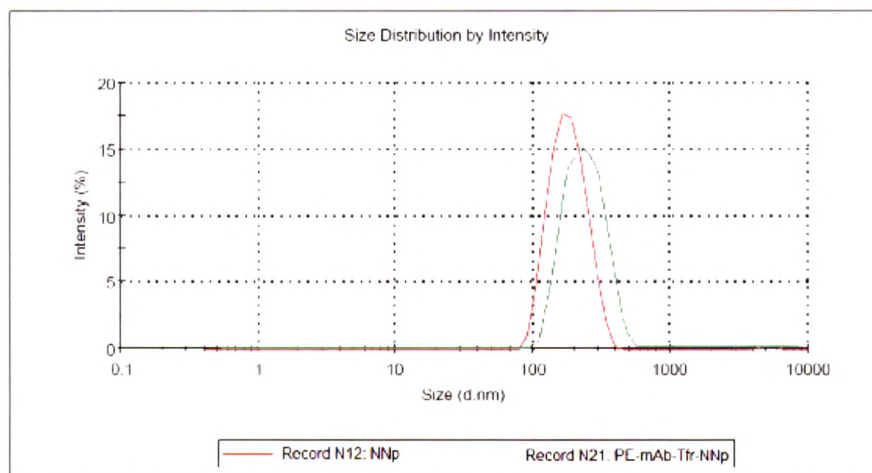
Figure 4.10: Zeta potential plot of nicergoline nanoparticles before and after antibody conjugation
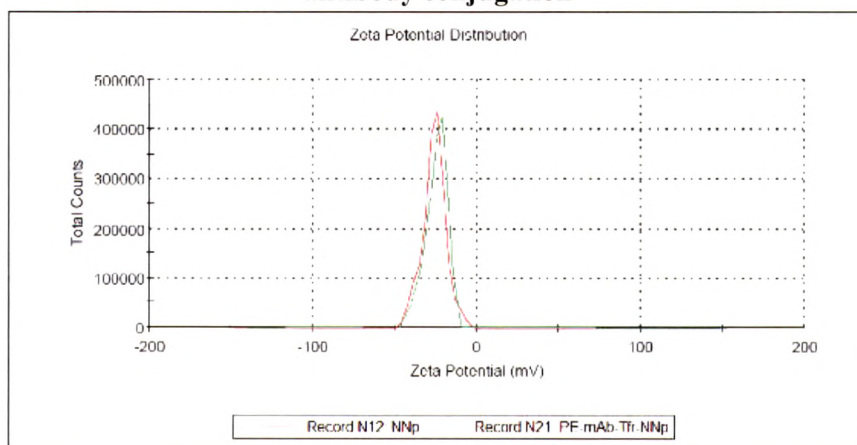
Figure 4.11: Particle size distribution plot of hydergine nanoparticles before and after antibody conjugation
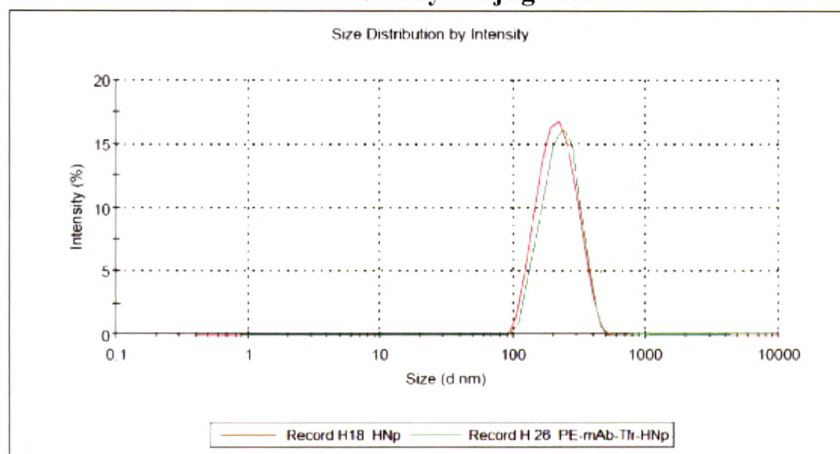
**Figure 4.12: Zeta potential plot of hydergine nanoparticles before and after antibody conjugation**
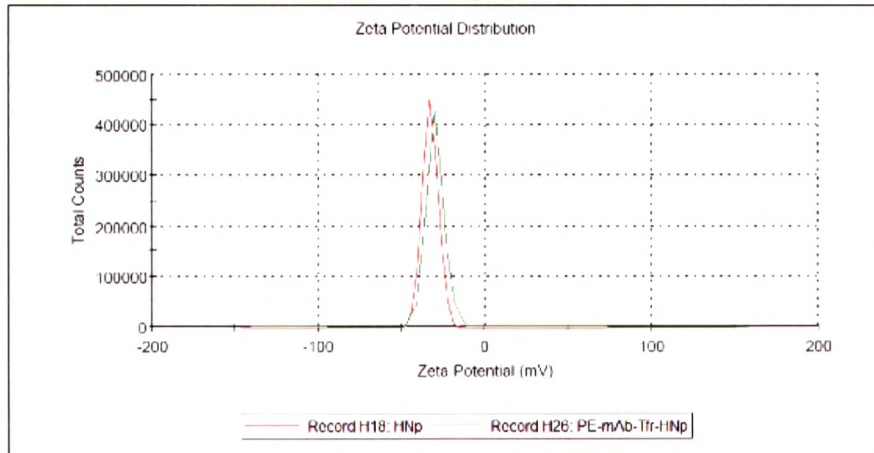
Figure 4.13: Particle size distribution plot of sibutramine nanoparticles before and after antibody conjugation
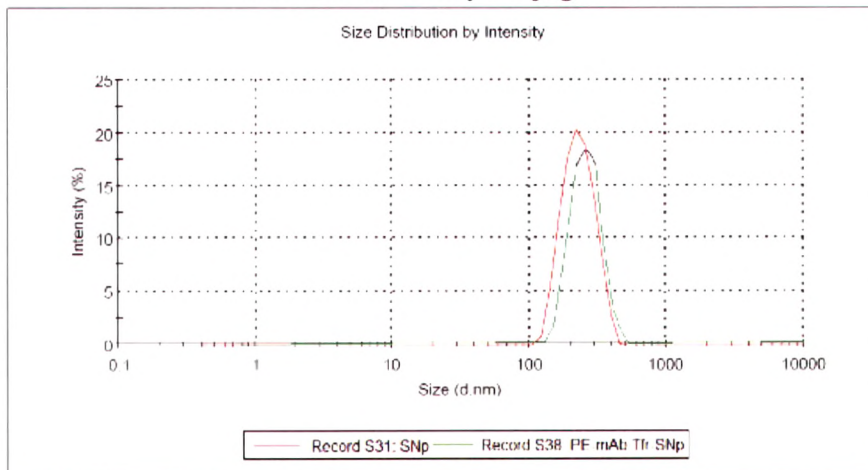
Figure 4.14: Zeta potential plot of sibutramine nanoparticles before and after antibody conjugation
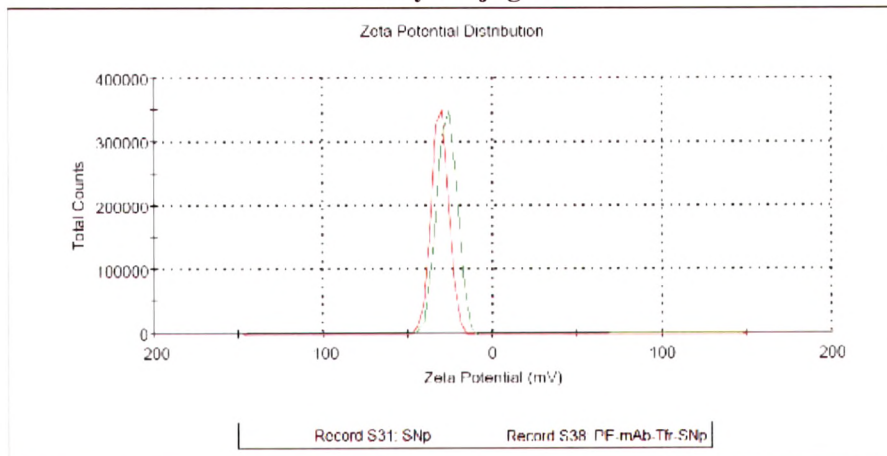
Table 4.23:- In-vitro diffusion study data for drug containing formulations

| Time (days)	Root time (min)	Cumulative percentage drug diffused (%w/w)					
Batch→		NNp	PE-mAb-Tfr-NNp	HNp	PE-mAb-Tfr-HNp	SNp	PE-mAb-Tfr-SNp
0	0	0	0	0	0	0	0
0.5	0	25.13 ± 1.27	8.53 ± 1.42	27.61 ± 2.03	7.52 ± 0.98	24.38 ± 1.54	8.06 ± 1.24
1	0.707	29.28 ± 1.11	14.95 ± 1.53	31.47 ± 1.62	13.04 ± 1.12	28.74 ± 1.17	12.78 ± 0.87
3	1	38.53 ± 2.06	23.53 ± 0.84	40.52 ± 0.94	21.67 ± 0.83	36.51 ± 2.03	21.26 ± 1.75
6	1.732	46.59 ± 1.07	31.15 ± 1.15	47.63 ± 1.36	29.16 ± 0.93	43.48 ± 0.98	30.48 ± 1.43
9	2.449	52.17 ± 1.34	40.27 ± 2.05	54.12 ± 2.09	36.25 ± 0.57	51.19 ± 1.26	38.62 ± 0.96
12	3	58.74 ± 2.06	48.49 ± 1.36	59.96 ± 1.07	43.48 ± 0.67	58.46 ± 1.52	46.91 ± 2.05
15	3.464	65.35 ± 0.94	56.57 ± 1.19	65.28 ± 0.85	50.82 ± 0.97	65.82 ± 0.83	54.56 ± 1.58
18	3.872	71.27 ± 1.03	63.41 ± 1.52	70.74 ± 1.87	58.11 ± 1.05	72.56 ± 1.28	63.21 ± 1.39
21	4.242	77.93 ± 1.09	70.86 ± 1.03	77.63 ± 2.14	67.23 ± 0.89	80.19 ± 1.71	71.83 ± 1.77
24	4.5826	85.46 ± 2.3	78.34 ± 2.3	83.17 ± 1.58	75.57 ± 2.8	87.13 ± 2.01	81.23 ± 1.42
Flux [(%w/w)/day]							
		2.787 ± 0.218	2.995 ± 0.325	2.652 ± 0.318	2.848 ± 0.209	2.92 ± 0.331	3.102 ± 0.194
R^2 values for different kinetic models							
Zero order		0.893 ± 0.013	0.973 ± 0.011	0.865 ± 0.017	0.979 ± 0.009	0.916 ± 0.029	0.978 ± 0.012
First order		0.41 ± 0.009	0.609 ± 0.034	0.384 ± 0.038	0.631 ± 0.037	0.43 ± 0.034	0.642 ± 0.026
Higuchi's kinetics		0.973 ± 0.018	0.988 ± 0.008	0.962 ± 0.021	0.979 ± 0.02	0.975 ± 0.011	0.984 ± 0.013

Figure 4.15: In-vitro diffusion study data for drug containing formulations

142
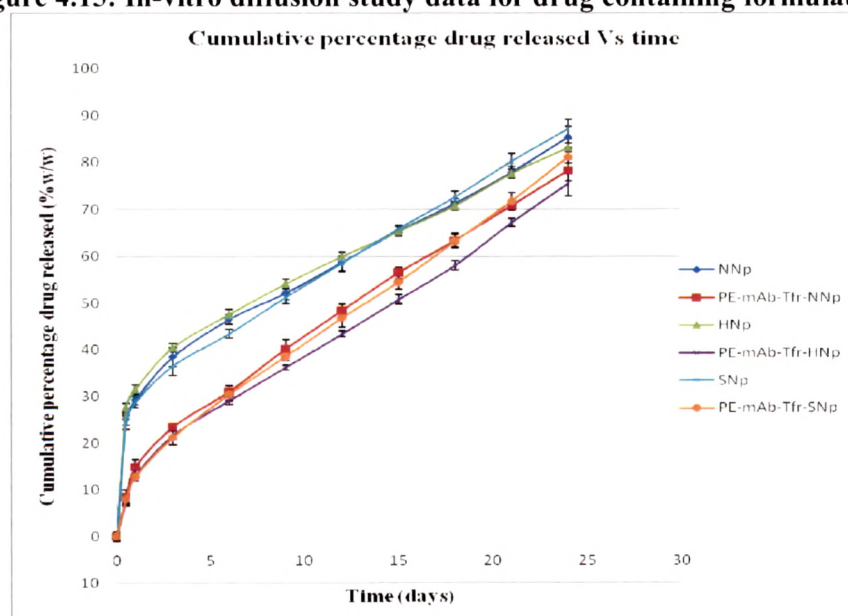
**Figure 4.16: Morphology of [A] NNp [B] PE-mAb-Tfr-NNp using TEM**
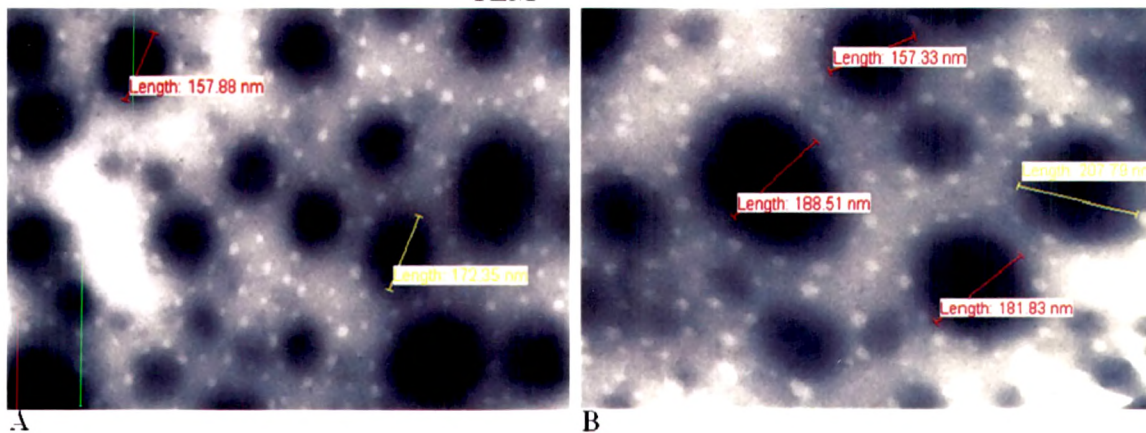
Figure 4.17: Morphology of [A] HNp [B] PE-mAb-Tfr-HNp using TEM
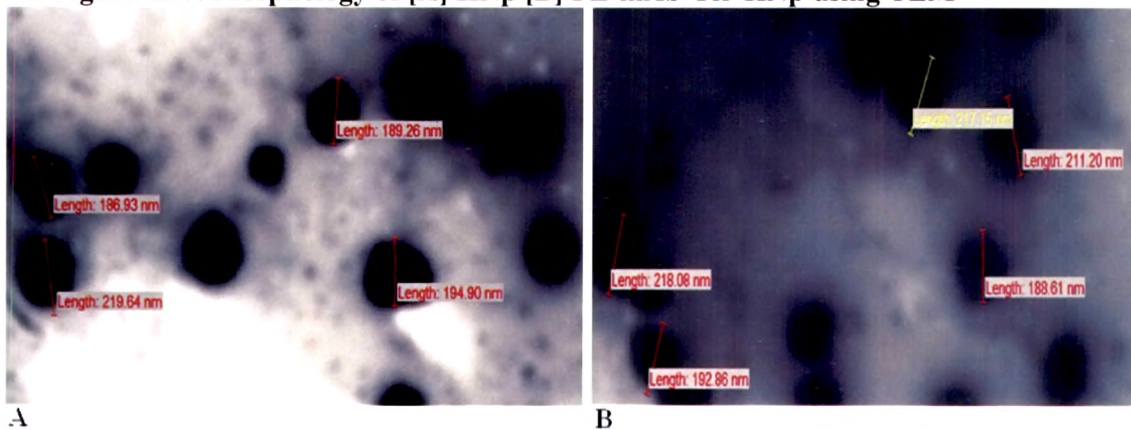

**Figure 4.18: Morphology of [A] SNp [B] PE-mAb-Tfr-SNp using TEM**
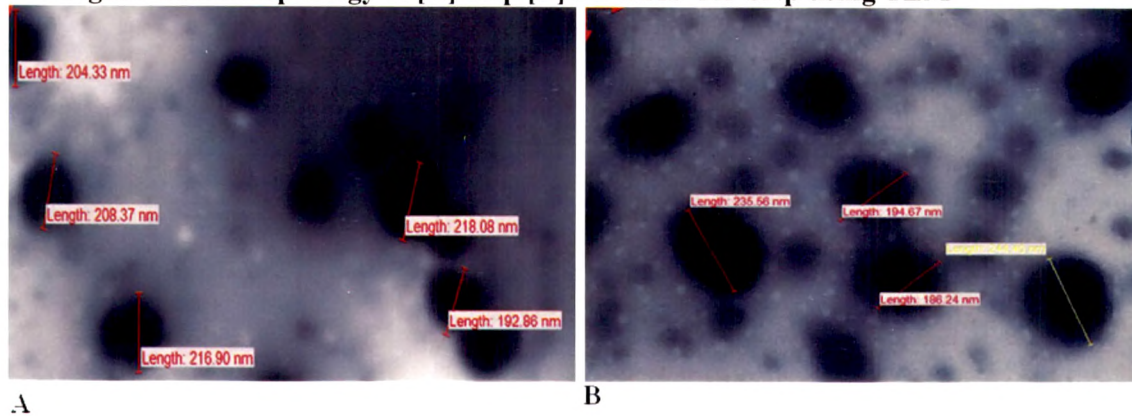
**Figure 4.19: DSC thermograms of [A] PLGA [B] NG [C] NNp**
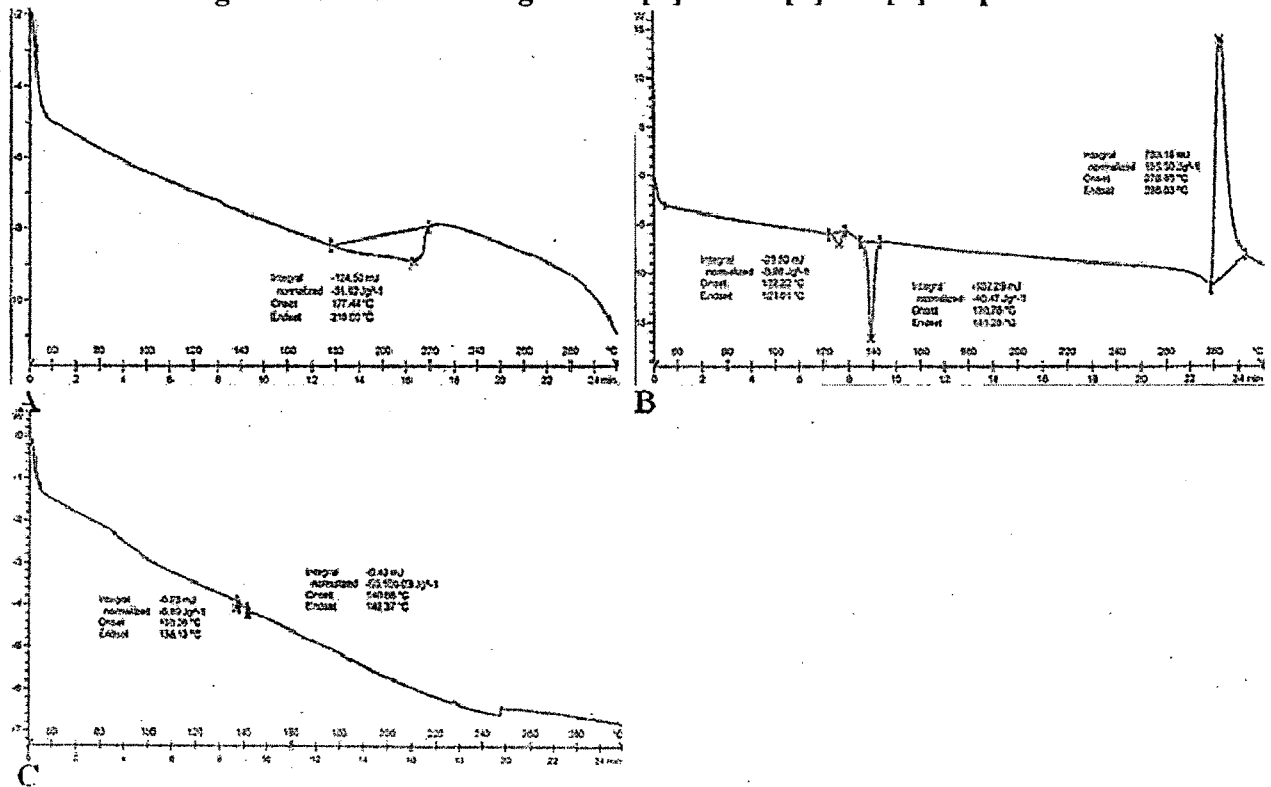
**Figure 4.20: DSC thermograms of [A] PLGA [B] HG [C] HNp**
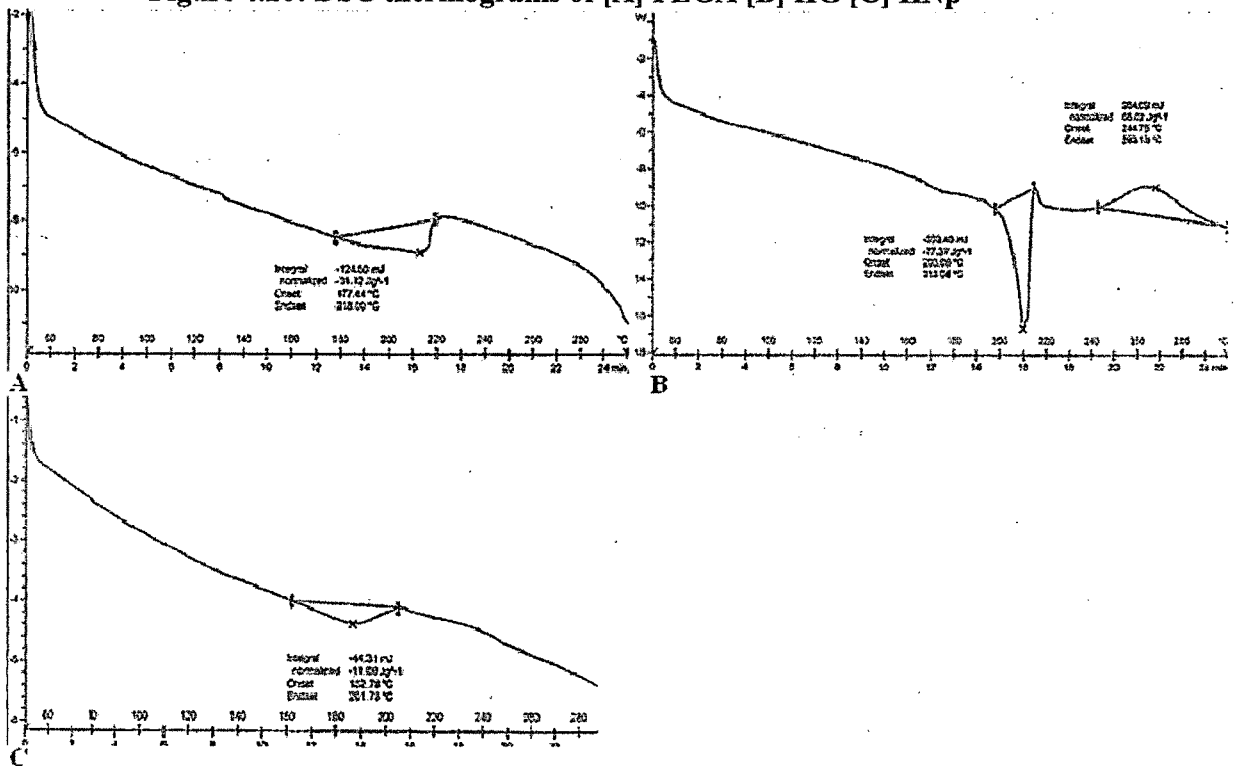
**Figure 4.21: DSC thermograms of [A] PLGA [B] SBMH [C] SB [D] SNp**
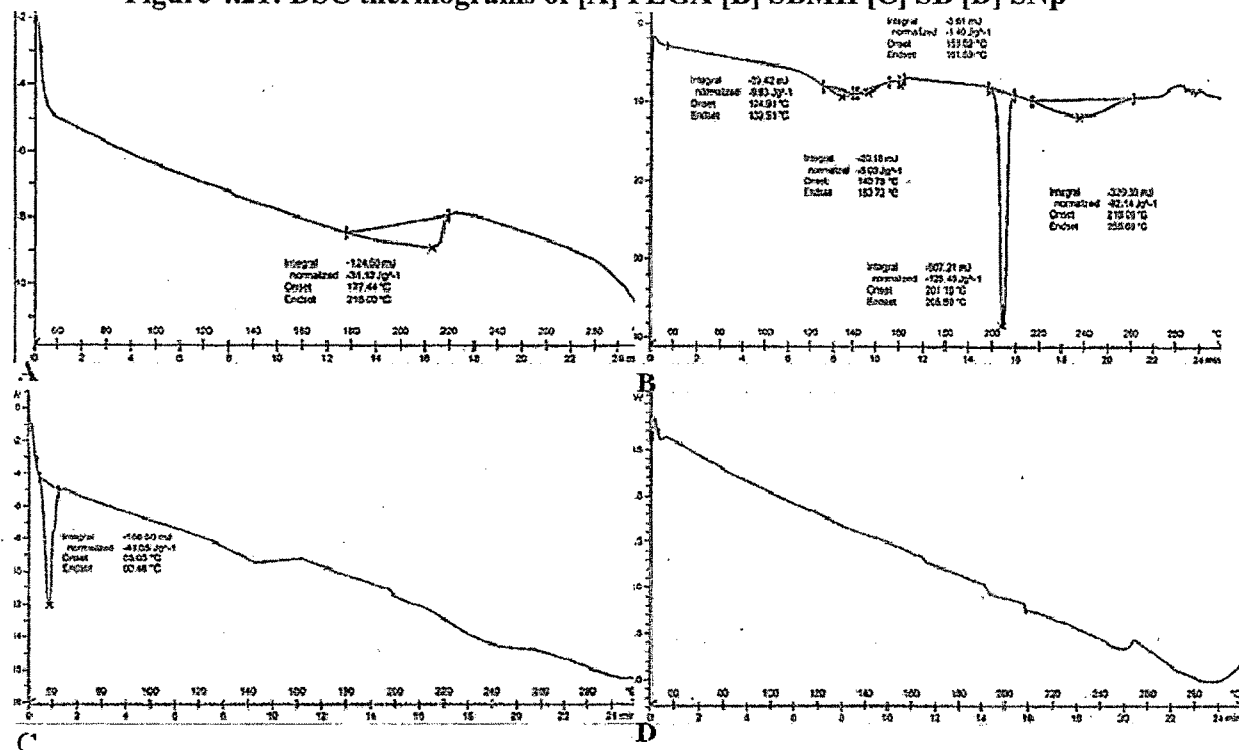
Table 4.24: Stability study data of nicergoline nanoparticles

Stability conditions	Description & Redispersibility	Particle size (nm)	Zeta potential (mV)	Drug content (%)	Particle size (nm)	Zeta potential (mV)	Drug content (%)
---	---	NNp			PE-mAb-Tfr-NNp		
Initial	Free flowing white powder with easy redispersibility	179.5 ± 6.2	-26.8 ± 1.8	102.5 ± 1.3	194.7 ± 4.3	-27.9 ± 1.8	100.9 ± 1.2*
		5°C ± 3°C					
1 M	Free flowing white powder with easy redispersibility	181.7 ± 6.4	-24.5 ± 1.4	101.6 ± 0.9	196.5 ± 4.8	-27.9 ± 1.1	99.1 ± 2.5
3 M	Free flowing white powder with easy redispersibility	185.2 ± 5.3	-23.6 ± 1.1	100.2 ± 1.4	200.3 ± 5.4	-26.3 ± 1.4	98.9 ± 2.1
6 M	Free flowing white powder with easy	190.3 ± 5.8	-22.1 ±	98.9 ±	204.1 ± 6.1	-25.6 ± 1.2	96.2± 1.9

145

			1.5	1.1			
redispersibility							
25°C ± 2°C/60% RH ± 5% RH							
1 M	Free flowing white powder with easy redispersibility	183.7 ± 4	-27.4 ± 0.9	99.6 ± 1.0	200.8 ± 4.6	-25.2 ± 1.3	98.7± 2.0
2 M	Free flowing white powder with easy redispersibility	236.5 ± 8	-24.1 ± 1.6	96.2 ± 1.3	238.2 ± 5.1	-21.9 ± 1.5	95.2± 2.3
3 M	White powder with poor flow and difficult redispersibility	278.3 ± 9	-20.8 ± 1.1	92.7 ± 1.1	281.7 ± 4.7	-17.4 ± 0.9	91.8± 1.8
6 M	White powder with poor flow and poor redispersibility	329.2 ± 6	-16.4 ± 1.5	88.4 ± 1.5	335.7 ± 5.3	-12.7 ± 1.3	87.4 ± 2.6

* Initial drug content was labeled as 100% and the drug content at different time points are with respect to the initial drug content

Table 4.25: Stability data of hydergine nanoparticles

Stability conditions	Description & Redispersibility	Particle size (nm)	Zeta potential (mV)	Drug content (%)	Particle size (nm)	Zeta potential (mV)	Drug content (%)
---	----	**HNp**			**PE-mAb-Tfr-HNp**		
Initial	Free flowing white powder with easy redispersibility	201.6 ± 5.7	-30.8 ± 4	102.5 ± 1.4	208.2 ± 5.3	-28.6 ± 3.1	100.6 ± 1.5*
5°C ± 3°C							
1 M	Free flowing white powder with easy redispersibility	203.4 ± 4.4	-30.1 ± 1.2	101.7 ± 0.9	209.5 ± 4.1	-27.7 ± 1.0	99.5 ± 1.2
3 M	Free flowing white powder with easy redispersibility	205.2 ± 5.1	-29.5 ± 1.4	100.8 ± 1.3	212.7 ± 3.9	-26.5 ± 1.1	98.1 ± 0.9
6 M	Free flowing white powder with easy redispersibility	210.3 ± 5.6	-28.3 ± 1.3	99.4 ± 1.0	217.1 ± 4.7	-25.3 ± 1.3	96.8± 1.3
25°C ± 2°C/60% RH ± 5% RH							

146

Stability conditions	Description & Redispersibility	Particle size (nm)	Zeta potential (mV)	Drug content (%)	Particle size (nm)	Zeta potential (mV)	Drug content (%)
1 M	Free flowing white powder with easy redispersibility	205.7 ± 3.9	-28.7 ± 1.4	100.7 ± 1.0	214.2 ± 4.1	-26.1 ± 1.0	99.1 ± 1.4
2 M	Free flowing white powder with easy redispersibility	221.9 ± 4.7	-25.4 ± 0.9	97.5 ± 1.3	227.6 ± 3.9	-23.2 ± 1.3	96.5 ± 2.1
3 M	White powder with poor flow and difficult redispersibility	248.3 ± 5.2	-20.8 ± 1.1	93.2 ± 1.1	256.7 ± 5.1	-19.7 ± 0.9	92.8 ± 1.3
6 M	White powder with poor flow and poor redispersibility	296.2 ± 3.8	-16.4 ± 1.5	89.6 ± 1.5	302.7 ± 4.6	-14.7 ± 0.7	88.7 ± 1.6

Table 4.26: Stability data of sibutramine nanoparticles

Stability conditions	Description & Redispersibility	Particle size (nm)	Zeta potential (mV)	Drug content (%)	Particle size (nm)	Zeta potential (mV)	Drug content (%)
---	---	SNp			PE-mAb-Tfr-SNp		
Initial	Free flowing white powder with easy redispersibility	210 ± 13	-26.5 ± 1.3	102.5 ± 1.1	218.4 ± 5.2	-23.8 ± 1.1	101.2 ± 0.9*
5°C ± 3°C							
1 M	Free flowing white powder with easy redispersibility	212.3 ± 5.4	-25.7 ± 0.9	101.9 ± 1.0	219.3 ± 4.6	-23.1 ± 1.5	100.4 ± 1.3
3 M	Free flowing white powder with easy redispersibility	215.7 ± 4.6	-24.3 ± 1.1	100.5 ± 0.9	220.1 ± 4.9	-23.6 ± 1.3	98.9 ± 1.7
6 M	Free flowing white powder with easy redispersibility	219.7 ± 5.8	-23.4 ± 1.5	99.3 ± 1.1	222.4 ± 5.1	-23.6 ± 1.0	99.2± 1.1
25°C ± 2°C/60% RH ± 5% RH							
1 M	Free flowing white powder with easy redispersibility	215.7 ± 4.1	-24.9 ± 1.2	100.3 ± 1.0	225.9 ± 5.7	-22.1 ± 1.3	99.7 ± 1.0

2 M	Free flowing white powder with easy redispersibility	230.5 ± 5.8	-22.1 ± 1.6	97.5 ± 1.3	239.6 ± 5.2	-18.9 ± 1.5	96.2 ± 1.3
3 M	White powder with poor flow and difficult redispersibility	251.4 ± 4.9	-19.6 ± 1.1	94.3 ± 1.1	281.7 ± 4.6	-15.6 ± 0.9	92.5 ± 1.8
6 M	White powder with poor flow and poor redispersibility	324.8 ± 5.5	-15.9 ± 1.5	90.1 ± 1.5	335.7 ± 4.5	-12.3 ± 1.3	88.4 ± 2.6

The residual dichloromethane and chloroform were 140±8ppm and 80±7ppm, and 25±4ppm and 10±2ppm for unconjugated and antibody conjugated NG and HG nanoparticles respectively.

4.3 Discussion

4.3.1 Precipitation of sibutramine base (SB) from Sibutramine hydrochloride monohydrate (SBHM) salt

SBHM was successfully converted into sibutramine base in high proportion and supported by the melting point determination and DSC thermograms without any SBHM present as an impurity.

4.3.2 Preparation and optimization of nanoparticles

The drug loaded nanoparticles were successfully prepared by the emulsion solvent evaporation technique with surfaced modified using mouse anti-transferrin receptor monoclonal antibody by carbodiimide method. Antibody conjugation efficiency was found to be more than 40% (400μg/mg of nanoparticles), much higher than the one reported so far (Aktas et al 2005, Kocbek et al 2007).

In this study, the main parameters affecting the nanoparticle formulation were found to be drug to polymer ratio per mL of organic phase (keeping the amount of the drug constant and represented as polymer to drug ratio), Lutrol F-68 total concentration (i.e in primary + secondary aqueous phase; keeping the volume of the organic phase constant) and organic to aqueous phase volume (primary + secondary aqueous phase; keeping the volume of the organic phase constant). Hence, were selected as independent variables to find the optimized condition for small particle size (PS)

148

(<225nm) and highest percentage drug entrapment efficiency (%EE) using 3^3 factorial design.

For intranasal administration, a wider particle size range (100-300nm) has been reported for polymeric nanoparticles for efficient drug delivery to the brain and brain transport has been found to be inversely proportional to the particle size. In this study, the particle size cut off was fixed as 225nm to have maximum drug entrapment to accommodate nanoparticles equivalent to the dose of the drug in small intranasally administrable volume of 300μL. Hence, the optimization criteria for particle size of drug loaded nanoparticles was kept as <225nm with highest percentage drug entrapment efficiency such that PS on antibody conjugation remains below 250nm.

Influence of the drug to polymer ratio

For all the three drug nanoparticles, the increase in the concentration of PLGA resulted in the increase in the particle size of the nanoparticles. The viscosity of the organic phase in which the PLGA is dissolved appears to affecting the nanoparticles size due to hindrance in rapid dispersion of PLGA solution into the aqueous phase and resulted increase in the droplet and nanoparticle size. (Chorny et al 2002) Availability of Lutrol F-68 on the surface of nanoparticles prevents the aggregation of nanoparticles during solvent evaporation but due to higher PLGA concentration, deposition of Lutrol F-68 on the particle surface may not be uniform and sufficient leading to aggregation. Increase in concentration of PLGA increases the drug entrapment efficiency for all the three drugs. It may be due to increase in drug entrapping polymer leading to a decrease in the diffusion of the drug towards the aqueous phase. (Song et al 2008 a, b).

Influence of Lutrol F-68 concentration

The particle size and drug entrapment efficiency were found to be inversely proportional to the surfactant Lutrol F-68 concentration. As the surfactant concentration was increased, the particle size and drug entrapment efficiency decreased for the drugs. The increase in the surfactant concentration leads to finer droplets and uniform distribution of the organic phase in the aqueous microenvironment resulting in smaller nanoparticles. Also, due to increased surfactant concentration the drug is available solubilized in the aqueous phase due to the

solubility enhancing effect of the surfactant with lesser drug available for encapsulation into the polymeric nanoparticles.

Influence of the organic: aqueous phase ratio

The particle size and drug entrapment efficiency were found to be inversely proportional to the organic: aqueous phase ratio. As the organic: aqueous phase ratio was increased, the particle size and drug entrapment efficiency decreased for the drugs. The increase in the organic phase ratio leads increased evaporation time causing slower polymer precipitation, due to the increased microenvironment provided by organic phase after dispersing in the aqueous phase, and thereby formation of small particles. Due to the increased evaporation time and slower polymer precipitation, the tendency of the drug to escape in the aqueous phase before polymer precipitation increases leading to lower drug entrapment efficiency.

Multiple regression analysis

Twenty-seven batches for each of the drug (NG, HG and SB) nanoparticles were prepared by emulsion solvent evaporation technique using 3^3 factorial design varying three independent variables namely drug to polymer ratio (X_1), Lutrol F-68 concentration (X_2) & organic to aqueous phase ratio (X_3). The influence of these independent variables on the dependent variables particle size (PS) and percentage drug entrapment efficiency (%EE) was evaluated and the results recorded in tables 4.7, 4.8 and 4.9 for NG, HG and SB nanoparticles respectively.

The PS and %EE obtained at various levels of three independent variables (X_1, X_2 and X_3) were subjected to multiple regression. Second order polynomial equations (full model) were obtained.

The effects of X_1, X_2 and X_3 on PS and % EE were evaluated by changing one variable at a time from its low to high value. The interactions (X_1X_2, X_1X_3, X_2X_3 and $X_1X_2X_3$) show how the particle size and entrapment efficiency changes when two or more variables were simultaneously changed.

For nicergoline, the particle size and entrapment values for the 27 batches showed a wide variation starting from a minimum of 124.3nm to maximum of 273.1nm and minimum of 70.2% to maximum of 85.4% respectively as shown in table 4.7. The

coefficients of terms X_1^2, X_1X_2, X_1X_3 X_2X_3, and $X_1X_2X_3$ ($p>0.05$) in equation 2 are regarded as least contributing to the PS of NNp. Similarly, the coefficients of terms X_1^2, X_3^2, X_1X_2, X_1X_3, X_2X_3 and $X_1X_2X_3$ (having $p>0.05$) in equation 3 are regarded as least contributing to the %EE of NNp. Hence, these terms were neglected from full model considering non-significant and reduced polynomial equation 8 and equation 9 were obtained for PS and %EE by including significant terms ($p<0.05$) of equation 2 and equation 3 respectively.

F-statistic of the results of ANOVA of full model and reduced model (as represented in table 4.11) confirmed omission of non-significant terms of equation 2 and equation 3. Since Fcal (0.6196) < Ftab (2.571) for PS and Fcal (0.989) < Ftab (2.447) for %EE ($a = 0.05$, $v_1 = 5$ and $v_2 = 6$), it was concluded that the neglected terms do not significantly contribute in predicting particle size and entrapment efficiency. When the coefficient values of three independent key variables (X_1, X_2, & X_3) in equation 8 and equation 9 were compared, the value for variable X_3 ($b_1 = 34.60312$ for particle size, $b_1 = 3.814683$ for entrapment efficiency) was found to be maximum and hence the variable X_3 was considered to be a major contributing variable for particle size and entrapment efficiency of NNp.

Similarly, for hydergine the PS and %EE values for the 27 batches ranged from minimum of 159.7nm to maximum of 301.6nm and minimum of 48.3% to maximum of 69.7% respectively as shown in table 4.8. The coefficients of terms X_1^2, X_3^2, X_1X_2, X_1X_3 and $X_1X_2X_3$ ($p>0.05$) in equation 4 are regarded as least contributing to the particle size of HNp. Similarly, the coefficients of terms X_1^2, X_2^2, X_1X_2, X_1X_3, X_2X_3 and $X_1X_2X_3$ (having $p>0.05$) in equation 5 are regarded as least contributing to the entrapment efficiency of HNp. Hence, these terms were neglected from full model considering non-significant and reduced polynomial equation 10 and equation 11 were obtained for PS and %EE by including significant terms ($p<0.05$) of equation 4 and equation 5 respectively.

F-statistic of the results of ANOVA of full model and reduced model (as represented in table 4.11) confirmed omission of non-significant terms of equation 4 and equation 5. Since Fcal (0.6196) < Ftab (2.571) for PS and Fcal (0.989) < Ftab (2.447) for %EE ($a = 0.05$, $v_1 = 5$ and $v_2 = 6$), it was concluded that the neglected terms do not

significantly contribute in predicting particle size and entrapment efficiency. When the coefficient values of three independent key variables (X_1, X_2, & X_3) in equation 10 and equation 11 were compared, the value for variable X_3 (b_1 = 11.19533 for particle size, b_2 = 2.996429 for entrapment efficiency) was found to be maximum and hence the variable X_3 was considered to be a major contributing variable for particle size and entrapment efficiency of HNp.

Similarly, for sibutramine base the PS and %EE values for the 27 batches ranged from minimum of 138.6nm to maximum of 310.1nm and minimum of 49.3% to maximum of 68.8% respectively as shown in table 4.9. The coefficients of terms X_1^2, X_2^2, X_1X_2, X_1X_3, X_2X_3 and $X_1X_2X_3$ (p>0.05) in equation 6 are regarded as least contributing to the particle size of SNp. Similarly, the coefficients of terms X_1^2, X_3^2, X_1X_2, X_1X_3, X_2X_3 and $X_1X_2X_3$ (having p>0.05) in equation 7 are regarded as least contributing to the entrapment efficiency of SNp. Hence, these terms were neglected from full model considering non-significant and reduced polynomial equation 12 and equation 13 were obtained for PS and %EE by including significant terms (p<0.05) of equation 6 and equation 7 respectively.

F-statistic of the results of ANOVA of full model and reduced model (as represented in table 4.12) confirmed omission of non-significant terms of equation 6 and equation 7. Since Fcal (0.7566) < Ftab (2.571) for PS and Fcal (2.316) < Ftab (2.447) for %EE (a = 0.05, v_1 = 5 and v_2 = 6), it was concluded that the neglected terms do not significantly contribute in predicting particle size and entrapment efficiency. When the coefficient values of three independent key variables (X_1, X_2, & X_3) in equation 12 and equation 13 were compared, the value for variable X_3 (b_1 = 17.59444 for particle size, b_2 = 2.684921 for entrapment efficiency) was found to be maximum and hence the variable X_3 was considered to be a major contributing variable for particle size and entrapment efficiency of HNp.

Contours

By keeping the major contributing independent variable fixed at -1, 0, +1 the contours were constructed between the other independent variables for particle size and drug entrapment efficiency separately.

For NNp, two dimensional contour plots for particle size and drug entrapment efficiency, from the reduced model based on equation 6 and equation 7, are shown in figures 4.2a, 4.2b, 4.2c and figures 4.3a, 4.3b, 4.3c respectively. The independent variable with highest coefficient was X_3 (polymer to drug weight ratio) for both particle size and drug entrapment efficiency.

Similarly, two dimensional contour plots for particle size and drug entrapment efficiency for HNp and SNp, from the reduced model based on equation 8 and equation 9, are shown in figures 4.4a, 4.4b, 4.4c and figures 4.5a, 4.5b, 4.5c, and figures 4.6a, 4.6b, 4.6c and figures 4.7a, 4.7b, 4.7c respectively. The independent variable with highest coefficient was X_3 (polymer to drug weight ratio) for both particle size and drug entrapment efficiency.

Check Point Analysis

For NNp, at fixed levels of -1, 0 and 1 of independent variable X_3, three check points were selected one each on three plotted contours. Nanoparticles at these three checkpoints were prepared experimentally using the same procedure keeping the other process variables as constant, with the amounts of X_1 and X_2 at the selected check points. The computed values from the contours at -1, 0 and 1 level and the experimentally determined values for particle size and drug entrapment efficiency values are shown in Table 4.13. Both experimentally obtained and theoretically computed particle size and entrapment efficiency values were compared using student 't' test and the difference was found to be non significant (p>0.05).

Similarly for HNp, the check point batches were selected from contours plotted at fixed levels of -1, 0 and 1 of independent variable X_3 (for particle size and drug entrapment efficiency). The computed values from contours and the experimental values are recorded in Table 4.14 for particle size and drug entrapment efficiency and the difference was found to be non significant (p>0.05).

Similarly for SNp, the check point batches were selected from contours plotted at fixed levels of -1, 0 and 1 of independent variable X_3 (for particle size and drug entrapment efficiency). The computed values from contours and the experimental

153

values are recorded in Table 4.15 for particle size and drug entrapment efficiency and the difference was found to be non significant ($p > 0.05$).

This proves the role of a derived reduced polynomial equation and contour plots in the preparation of nanoparticles of NG, HG and SB of predetermined particle size and drug entrapment efficiency within the selected range of the independent variables.

Optimized batches

For NG, the batch with particle size of 173.6 ± 6.1nm and drug entrapment efficiency of 81.2 ± 2.1% prepared at 0 level of X_1 (30mL of aqueous phase per mL of organic phase), 0 level of X_2 (total 0.32%w/v Lutrol F-68 in aqueous phase) and 0 level of X_3 (20:1 polymer to drug weight ratio) was considered optimum based on the criteria of particle size <225nm with highest drug entrapment efficiency. Hence, 4mg of drug and 80mg of PLGA were dissolved in 1ml of dichloroform and emulsified with 4 mL aqueous solution of 1.5%w/v lutrol F-68 and 0.5%w/v PVA, and this primary emulsion was added dropwise to 30mL of 0.11%w/v lutrol F-68 aqueous solution under constant stirring.

Similarly for HG, the batch with 198.6 ± 5.3nm particle size and 65.8 ± 1.3% drug entrapment efficiency was considered to be optimum at 0 level of X_1 (30mL of aqueous phase per mL of organic phase), 0 level of X_2 (total 0.32%w/v Lutrol F-68 in aqueous phase) and 0 level of X_3 (20:1 polymer to drug weight ratio). And for SB, the batch with 210.3 ± 5.7nm particle size and 62.5 ± 1.5% drug entrapment efficiency was considered to be optimum at 0 level of X_1 (30mL of aqueous phase per mL of organic phase), 0 level of X_2 (total 0.32%w/v Lutrol F-68 in aqueous phase) and 0 level of X_3 (20:1 polymer to drug weight ratio).

4.3.3 Lyophilization and optimization of cryoprotectant concentration

Freeze-drying has been the most utilized drying method for nanoparticle suspensions. Since, freeze-drying is a highly stressful process for nanoparticles, addition of cryoprotectants become essential. For nanoparticles carbohydrates have been perceived to be suitable freeze-drying protectants. There are considerable differences in the cryoprotective abilities of different carbohydrates.

The optimized batch of nanoparticles was lyophilized using sucrose, mannitol and trehalose (at 1:2, 1:3 and 1:4 nanoparticle to cryoprotectant) to select suitable cryoprotectant and its concentration. The redispersibility of the freeze-dried formulations and particle size of the nanoparticles before and after freeze-drying were evaluated and recorded in table 4.16.

With the use of sucrose as cryoprotectant, the cake formed after lyophilization was found to be of condensed and collapsed structure. Hence, the redispersibility of nanoparticles was poor and was only possible with sonication. For the different ratios of 1:2, 1:3 and 1:4 nanoparticle sizes, as shown in table 4.16, increased significantly after lyophilization. The S_f/S_i values were 3.25, 2.53 and 2.27 with 1:2, 1:3 and 1:4 NPs to sucrose respectively. The increase in the particle size could have been due to the cohesive nature of the cryoprotectant. Further, it was observed that the lyophilized nanoparticles with sucrose had tendency to absorb moisture quickly on uncapping.

While, with mannitol the lyophilized product was fluffy and snow like voluminous cake. Also, the nanoparticle formulation showed free flowing. However, the redispersibility of nanoparticles was difficult and possible only after vigorous shaking. The particle size, recorded in table 4.16, increased significantly after lyophilization than the initial. The S_f/S_i values were 2.32, 2.03 and 1.18 with 1:2, 1:3 and 1:4 NPs to mannitol respectively. This may be due to the low solubility of mannitol in water (0.18 parts of mannitol soluble in 1 part of water).

With trehalose also, the lyophilized nanoparticles formed fluffy and snow like voluminous cake. With trehalose as cryoprotectant, the lyophilized nanoparticles were redispersed easily and the increase in particle size was not significant as indicated by S_f/S_i values 1.7, 1.36, and 1.08 for 1:2, 1:3 and 1:4 NPs to trehalose respectively (table 4.16). The redispersion of the nanoparticles depends on the hydrophilicity of the surface. The easy redispersibility could be probably due to the higher solubility of trehalose in water (0.7 parts in 1 part of water). The cryoprotective effect may be attributed to the ability of trehalose to form a glassy amorphous matrix around the particles, preventing the particles from sticking together during removal of water

(Konan et al 2002). Also, the property of the tyndall effect observed with nanoparticles was retained after redispersion of the nanoparticles lyophilized using trehalose. Furthermore, trehalose, a non-reducing disaccharide of glucose, has previously demonstrated satisfactory cryoprotective effects for pharmaceutical and biological materials (De Jaeghere et al 1999).

Therefore, trehalose at a ratio of 1: 4 (nanoparticles: trehalose) was used as cryoprotectant for lyophilization of optimized batch of nanoparticles for further studies.

4.3.4 Antibody conjugation of nanoparticles

The surface modification of PLGA nanoparticles with antibody PE-mAb-Tfr was achieved in two steps using carbodiimide coupling method. This active ester method yields stable amide bonds. As a prerequisite, the polymer has to contain free carboxyl groups at the surface as represented by the H-type of PLGA which are activated by carbodiimide/N-hydroxysuccinimide. In contrast to the activation of carboxyls with only carbodiimide, the presence of N-hydroxysuccinimide yields N-hydroxysuccinimide esters as stable intermediates which rather acylate amino groups of proteins than to be subject of hydrolysis in aqueous medium (Staros et al 1986, Grabarek et al 1990). The activation pH, reaction temperature, activation time, amount of activating agents (EDC-HCl/NHS) and PE-mAb-Tfr to NPs ratio were optimized to achieve minimum particle size and maximum conjugation efficiency. The antibody conjugation efficiencies for PE-mAb-Tfr-NNp, PE-mAb-Tfr-HNp and PE-mAb-Tfr-SNp were found to be 43.5 ± 1.2, 42.6 ± 1.4 and 44.1 ± 1.1 which is much more times than the one reported in previous studies and may be attributed to the precise optimization of the various process parameters (Aktas et al 2005, Kocbek et al 2007).

The activation pH was varied between 5-7 and at acidic pH of 5 highest conjugation efficiency was observed with a concurrent decrease in %EE which may be due to accelerated hydrolysis of PLGA at this pH (table 4.17). EDC is generally used as a carboxyl activating agent in the 4.0-6.0 pH range and hence a low conjugation efficiency was observed at pH 7 followed by at pH 6. Hence, taking into account the conjugation efficiency and %EE, the activation pH was optimized as 5 for

nanoparticle activation followed by antibody conjugation effected at pH 7.4 to avoid denaturation of protein at lower pH. It was observed that the activation pH did not significantly affect the mean particle size of antibody conjugated nanoparticles.

The effect of temperature on antibody conjugation to nanoparticles was also evaluated and the results are recorded in table 4.18. At a reaction temperature of 45°C both the conjugation efficiency and %EE were observed to be the lowest which may be attributed to low glass transition temperature of PLGA of 45°C resulting in increased drug leaching from nanoparticles and availability of less surface carboxyl group to effect conjugation. The same may explain for a low conjugation efficiency and %EE at 30°C. Also, carbodiimide coupling has been reported to be efficient at room temperature. While both conjugation efficiency and %EE were observed to be high at a temperature of 15°C and hence, was optimized as reaction temperature.

The effect of the amount of activating agent (EDC-HCl/NHS concentration) on conjugation efficiency of antibody to nanoparticles was assessed and the results recorded in table 4.19. It was observed that increasing the concentration of activating agent from 7.3 to 7.8 μM there was an increase in conjugation efficiency from 29.9±1.6% to 40.9±2.3% with no appreciable effect on mean particle size or %EE of antibody conjugated nanoparticles. While, there was no significant increase in antibody conjugation efficiencies of nanoparticles with increase in EDC-HCl/NHS concentration from 7.8 to 8.3 μM indicating nanoparticle surface saturation with unavailability of surface carboxyl groups for more antibody attachment.

The influence of reaction time (activation and conjugation time) on conjugation efficiency of PE-mAb-Tfr to nanoparticles was also checked and the results are recorded in table 4.20. The conjugation efficiency of antibody to nanoparticles was observed to be significantly low with a reaction time of 1 hr (half an hour each for activation and conjugation) with no significant effect on particle size and %EE indicating the time to be insufficient to achieve maximum antibody conjugation. However, there was no significant increase in antibody conjugation, mean particle size and %EE with increase in reaction time from 2 to 3 hr. Thus, the reaction time was standardized as 2 hr.

The amount of antibody (PE-mAb-Tfr) was varied from 10µg to 500µg (table 4.21). For all the three drug nanoparticles, with increase in the amount of antibody the conjugation efficiency increased with no significant increase in particle size. This is because by increasing the antibody concentration from 10µg to 500µg no surface saturation was observed for PLGA nanoparticles with respect to the antibody attached as has not been used in molar ratios.

4.3.5 Characterization of nanoparticles

4.3.5.1 [^{1}H]NMR of the antibody conjugated nanoparticles

In figure 4.8 peak at 5.1 in NMR spectra of antibody conjugated NG nanoparticles (Figure 4.8[B]) with respect to unconjugated NG nanoparticles (Figure 4.8[A]) demonstrate antibody conjugation to the nanoparticles.

4.3.5.2 Particle size, zeta potential and drug entrapment efficiency

The particle size, zeta potential and drug entrapment efficiency (%EE) for drug loaded unconjugated nanoparticles and antibody conjugated drug loaded nanoparticles are recorded in table 4.22 and the particle size and zeta potential for the nanoparticles are shown graphically in figures 4.9 to 4.14. Increase in the particle size after antibody conjugation may be due to antibody conjugation to the surface of unconjugated nanoparticles. While, the increase in zeta potential may be due to screening of the negative charge because of the antibody conjugated to the nanoparticle surface. And the decrease in %EE may be explained by the accelerated leaching of the drug from the nanoparticles being subjected to different pH conditions during antibody conjugation.

4.3.5.3 In-vitro drug release

The release of the drug from PLGA is by the degradation of polymer by hydrolysis of its ester linkages in the presence of water. In general the mechanism by which active agent is released from a delivery vehicle is a combination of diffusion of the active agent from the polymer matrices, bulk erosion of the polymer, swelling and degradation of the polymer. The degradation of PLGA is slow, therefore the release of the drugs from the nanoparticles may depend on drug diffusion and PLGA surface

and bulk erosion or swelling. The results of in vitro for the drug NPs are tabulated in table 4.23 and shown graphically in figure 4.15.

For all the drug loaded unconjugated nanoparticles there was an initial burst release of more than 24% in 12hrs (0.5 days) and then there was a lag phase and more than 83% release in 21 days. This high initial burst from unconjugated nanoparticles can be attributed to the immediate dissociation and dissolution of drug adhered on the surface and located near the surface of the NPs (Magenheim et al., 1993). After that, in lag phase, the release is mainly due to the erosion of the polymer matrix and further diffusion of drug molecules through the polymeric matrix of the NPs. The matrix material would require time to erode in the aqueous environment than the release mechanisms of surface release, resulting in the prolonged release.

The burst effect was absent in antibody conjugated drug nanoparticles and the release in 21 days was found to be about 80%. The absence of burst release with antibody conjugated NPs may be due to absence of drug on the surface of conjugated NPs.

4.3.5.4 *Transmission electron microscopy*

The TEM images for drug containing unconjugated and antibody conjugated nanoparticles are shown in figure 4.16, 4.17 and 4.18 for NG, HG and SB nanoparticles respectively. TEM images of the unconjugated and conjugated NPs showed spherical NPs with smooth surfaces.

4.3.5.5 *Differential Scanning Calorimetry*

DSC studies were performed to investigate the physical state of the drug in the NPs, because this aspect could influence the in vitro and in vivo release of the drug from the systems. Different combinations of drug/polymer may coexist in the polymeric carriers, such as: (i) amorphous drug in either an amorphous or a crystalline polymer and (ii) crystalline drug in either an amorphous or a crystalline polymer. Moreover, a drug may be present either as a solid solution or solid dispersion in an amorphous or crystalline polymer. PLGA shows a Tg from 177.44 to 218.00°C (figure 4.19a) and not a Tm (melting point), indicating the presence of the polymer in amorphous form.

DSC thermogram of plain NG shown in figure 4.19b depicts a sharp melting peak from 136.76 to 141.26°C, indicating the crystalline nature of the drug. For NNp, as shown in figure 4.19c, the sharp drug peak of NG is absent indicating the conversion of NG into amorphous state during the nanoparticle formulation and thereby entrapped in the PLGA polymer.

DSC thermogram of plain HG shown in figure 4.20b depicts a sharp melting peak from 203.66 to 213.06°C, indicating the crystalline nature of the drug. For HNp, as shown in figure 4.20c, the peak of HG stretched from 182.78-201.78°C indicating the conversion of HG into amorphous state during the nanoparticle formulation and thereby entrapped in the PLGA polymer.

Figure 4.21b of SBHM shows a sharp peak from 201.16 to 205.59°C while DSC thermogram of plain SB shown in figure 4.21c depicts a sharp melting peak from 55.05 to 60.46°C, indicating the crystalline nature of the drug and complete conversion of SBHM into SB without SBHM as an impurity. For SNp, as shown in figure 4.21d, the sharp peak of SB is absent indicating the conversion of SB into amorphous state during the nanoparticle formulation and thereby entrapped in the PLGA polymer.

4.3.5.6 Stability studies

The stability studies of the formulations were performed in order to study the influence of varying environmental conditions on the parameters of the formulation influencing the therapeutic response. It was observed that for unconjugated and antibody conjugated nanoparticles of NG, HG and SB, no significant change (P>0.05) was observed in particle size, zeta potential and drug content at 5°C ± 3°C for 6M.

The storage of the unconjugated and antibody conjugated drug nanoparticles of the drugs at 25°C ± 2°C/60% ± 5% RH, led to an increase in the particle size. The increase in the particle size was not significant during the first month, however became significant and more prominent after 2, 3 and 6 months. The polydispersity index of the nanoparticle stored at 25°C ± 2°C/60% ± 5% RH was found to increase

as compared to the initial. The increase in the particle size may be due to the absorption of the moisture by the nanoparticles resulting in the coalescence of the small nanoparticles forming particles larger in size. The nanoparticles were also observed for physical appearance. After 3 and 6 months the physical appearance was also changed, with loss of the free flowing property followed by the difficulty in redispersibility.

At 25°C ± 2°C/60% ± 5% RH, the zeta potential of the nanoparticles shifted towards zero for both unconjugated and antibody conjugated drug nanoparticles. This may be due to the acidic conditions produced due to the degradation of PLGA into lactic and glycolic acid (Sahoo et al 2002). The lowered zeta potential values also might have contributed toward the aggregation of particles.

The drug content of the unconjugated and antibody conjugated drug nanoparticles was not altered up to 6M at 5°C ± 3°C. However, the drug content was reduced after 6M storage at 25°C ± 2°C/60% RH ± 5% RH. The drug content for HG nanoparticles was found to have significant impact, with the drug content reducing below 95% after 3M and 6M storage at 25°C ± 2°C/60% ± 5% RH. This impact could be due to the moisture absorbed by the nanoparticles upon storage at 25°C ± 2°C/60% RH ± 5% RH, possibly resulting in the degradation of the drug.

Thus the unconjugated and antibody conjugated PLGA nanoparticles of NG, HG and SB when stored at 25°C ± 2°C/60% RH ± 5% RH for 6M show instability reflected by change in physical appearance, increase in the particle size, zeta potential and reduction in the drug content. Hence, we can conclusively specify that both unconjugated and antibody conjugated nanoparticles of the three drugs were stable and can be stored 5°C ± 3°C for 6M retaining its original formulation characteristics.

4.3.5.7 Determination of residual dichloromethane/chloroform in nanoparticles

Residual dichloromethane/chloroform was found to be within the permissible limit for both unconjugated and antibody conjugated nanoparticles. Residual dichloromethane/chloroform of antibody conjugated nanoparticles was less than the unconjugated nanoparticles and can be due to the evaporation/washing of surface dichloromethane/chloroform during conjugation process.

4.4 CONCLUSION

PLGA nanoparticles of NG, HG and SB were successfully prepared by emulsion solvent evaporation method and surface modified with monoclonal antibody for selective brain drug delivery following intranasal administration. The particle observed for both unconjugated and antibody conjugated drug nanoparticles was below 250nm suitable for intranasal administration. The unconjugated and antibody conjugated drug nanoparticles were characterized and subjected to stability studies and were found to be stable and suitable for intranasal administration.

References

- Akta Y, Yemisci M, Andrieux K, Gürsoy RN, Alonso MJ, Fernandez-Megia E, Novoa-Carballal R, Quinoa E, Riguera R, Sargon MF, Celik HH, Demir AS, Hincal AA, Dalkara T, Capan Y, Couvreur P. Development and brain delivery of chitosan-PEG nanoparticles functionalized with the monoclonal antibody OX26. *Bioconjug Chem.*, 2005, 16(6), 1503-1511.

- Chorny M, Fishbein I, Haim D. Danenberg, Gershon Golomb. Lipophilic drug loaded nanospheres prepared by nanoprecipitation: effect of formulation variables on size, drug recovery and release kinetics. *Journal of Controlled Release*, 2002, 83, 389-400.

- Csaba N, Garcia-Fuentes M, Alonso MJ. Nanoparticles for nasal vaccination. *Adv Drug Deliv Rev.*, 2009, 61(2), 140-157.

- De Jaeghere F, Allemann E, Leroux JC, Stevels W, Feijen J, Doelker E, Gurny R. Formulation and lyoprotection of poly (lactic acid-co-ethylene oxide) nanoparticles: influence on physical stability and in vitro cell uptake. *Pharm. Res*, 1999, 16, 859-866.

- Feng SS. Nanoparticles of biodegradable polymers for new-concept chemotherapy. *Expert Reviews Medical Devices*, 2004, 1 (1), 115-125.

- Grabarek Z, Gergely J. Zero-length cross-linking procedure with the use of active esters. *Anal Biochem*, 1990, 185, 131-135.

- Guerrero DQ, Allemann E, Fessi H, Doelker E. Preparation techniques and mechanisms of formation of biodegradable nanoparticles from performed polymers. *Drug Dev. Ind. Pharm.*, 1998, 24 (12), 1113-1128.

- Jain RA. The manufacturing techniques of various drug loaded biodegradable poly(lactide-co-glycolide) devices. *Biomaterials*, 2000, 21, pp.2475-2490.

- Kocbek P, Obermajer N, Cegnar M, Kos J, Kristl J. Targeting cancer cells using PLGA nanoparticles surface modified with monoclonal antibody. *J Control Release*, 2007, 120(1-2), 18-26.

- Konan YN, Gurny R, et al. Preparation and characterization of sterile and freeze-dried sub-200nm nanoparticles. *Int J Pharm*, 2002, 233, 239-252.

- Labhasetwar V. Nanoparticles for drug delivery. *Pharm. News*, 1997, 4, pp.28-31.

- Langer R. Tissue engineering: a new field and its challenges. *Pharm. Res.*, 1997, 14 (7), pp.840-841.

- Levison KK, Takayama K, Isowa K, Okaba K, Nagai T. Formulation optimization of indomethacin gels containing a combination of three kinds of cyclic monoterpenes as percutaneous penetration enhancers. *J Pharm Sci.*, 1994, 83, 1367-1372.

- Minko T. Drug targeting to the colon with lectins and neoglycoconjugates. *Advanced Drug Deliv. Rev*, 2004, 56, 491-509.

- Misra A, Sheth AK. Mathematical modeling of preparation of acyclovir liposomes:reverse phase evaporation method. *J Pharm Pharmaceut Sci*, 2002, 5(3), 285-291.

- Moghimi SM, Hunter AC, Murray JC. Long-circulating and target specific nanoparticles: theory to practice. *Pharmacol. Rev.*, 2001, 53 (2), pp.283-318.

- Quintanar-Guerrero D, Allemann E, Fessi H, Doelker E. Preparation techniques and mechanisms of formation of biodegradable nanoparticles from preformed polymers. *Drug Dev Ind Pharm.*, 1998, 24(12), 1113-1128.

- Saez A, Guzman M, Molpeceres J, Aberturas MR. Freeze-drying of polycaprolactone and poly(D,L-lactic-glycolic) nanoparticles induce minor particle size changes affecting the oral pharmacokinetics of loaded drugs. *Eur. J. Pharm.Biopharm*, 2000, 50, 379-387.

- Sahoo SK, Panyam J, Prabha S, Labhasetwar V. Residual polyvinyl alcohol associated with poly (D,L-lactide-co-glycolide) nanoparticles affects their physical properties and cellular uptake. *Journal of Controlled Release*, 2002, 82, 105-114.

- Sahoo SK, Wenxue MA, Labhasetwar V. Efficacy of transferrin-conjugated paclitaxel-loaded Nanoparticles in a murine model of prostate cancer. *Int. J. Cancer*, 2004, 112, 335-340.

- Scholes PD, Coombes AGA, Illum L, *et al.* The preparation of sub-200 nm poly (lactide-co-glycolide) microspheres for site-specific drug delivery. *J Controlled Release*, 1993, 25, pp.145-153.

- Sharma A, Sharma S and Khuller GK. Lectin-functionalized poly (lactide-co-glycolide) nanoparticles as oral/aerosolized antitubercular drug carriers for treatment of tuberculosis. *Journal of Antimicrobial Chemotherapy*, 2004, 54, 761-766.

- Shirakura O, Yamada M, Hashimoto M, Ishimaru S, Takayama K, Nagai T. Particle size design using computer optimization technique. *Drug Dev Ind Pharm*, 1991, 17, 471-483.

- Song X, Yu Zhao, Hou S, Xu F, Zhao R, He J, Cai Z, Li Y, Chen Q. Dual agents loaded PLGA nanoparticles: systematic study of particle size and drug entrapment efficiency. *European Journal of pharmaceutics and biopharmaceutics*, 2008a, 69, 445-453.

- Song X, Yu Zhao, Wenbin Wu, Yueqi Bi, Zheng Cai, Qiuhong Chen, Yuanbo Li, Shixiang Hou. PLGA nanoparticles simultaneously loaded with vincristine sulfate and verapamil hydrochloride: Systematic study of particle size and drug entrapment efficiency. *International Journal of Pharmaceutics*, 2008b, 350, 320-329.

- Staros JV, Wright RW, Swingle DM. Enhancement by Nhydroxysulfosuccinimide of water-soluble carbodiimide-mediated coupling reactions. *Anal Biochem*, 1986, 156, 220-222.

- Stella B, Arpicco S, Peracchia MT, Desmaele D, Hoebeke J, Renoir M, D'Angelo J, Cattel L, Couvreur P. Design of folic-acid-conjugated nanoparticles for drug delivery. *Journal of Pharmaceutical Sciences*, 2000, 89 (11), 1452-1464.

- Zhang QZ, Zha LS, Zhang Y, Jiang WM, Lu W, Shi ZQ, Jiang XG, Fu SK. The brain targeting efficiency following nasally applied MPEG-PLA nanoparticles in rats. *J Drug Target.*, 2006, 14(5), 281-290.